3-9-2009

Production and Characterization of High Repetition Rate Terahertz Radiation in Femtosecond-Laser-Induced Air Plasma

Michael L. Dexter

PRODUCTION AND CHARACTERIZATION OF HIGH REPETITION RATE TERAHERTZ RADIATION IN FEMTOSECOND-LASER-INDUCED AIR PLASMA

THESIS

Michael L. Dexter, Captain, USAF
AFIT/GAP/ENP/09-M04

DEPARTMENT OF THE AIR FORCE
AIR UNIVERSITY

AIR FORCE INSTITUTE OF TECHNOLOGY

Wright-Patterson Air Force Base, Ohio

The views expressed in this thesis are those of the author and do not reflect the official policy or position of the United States Air Force, Department of Defense, or the United States Government.

AFIT/GAP/ENP/09-M04

PRODUCTION AND CHARACTERIZATION OF HIGH REPETITION RATE TERAHERTZ RADIATION IN FEMTOSECOND-LASER-INDUCED AIR PLASMA

THESIS

Presented to the Faculty

Department of Engineering Physics

Graduate School of Engineering and Management

Air Force Institute of Technology

Air University

Air Education and Training Command

In Partial Fulfillment of the Requirements for the

Degree of Master of Science in Applied Physics

Michael L. Dexter, BS

Captain, USAF

March 2009

AFIT/GAP/ENP/09-M04

PRODUCTION AND CHARACTERIZATION OF HIGH REPETITION RATE TERAHERTZ RADIATION IN FEMTOSECOND-LASER-INDUCED AIR PLASMA

Michael L. Dexter, BS
Captain, USAF

Approved:

Matthew J. Bohn (Chairman)	6 Mar 09 Date
Steven T. Fiorino (Member)	9 MAR 09 Date
Jason Deibel (Member)	3/5/09 Date

ABSTRACT

The purpose of this research was to produce and characterize high repetition rate terahertz radiation in ionized air plasma. An 800 nanometer, 50 femtosecond, 0.35 Watt, 40 KHz, pulsed Ti:Sapphire laser system was used as the source infrared beam. This beam was focused onto a second harmonic generation crystal to produce a collinear, perpendicularly polarized secondary beam at 400 nm. After realigning the polarization of the fundamental to the second harmonic and compensating for group velocity dispersion introduced by the optics, both beams were recombined and focused by a 3.75 cm focal length mirror to form an air plasma. An electrical bias of up to 27 kV/cm was applied across the plasma to enhance the terahertz and plasma signal. The air plasma intensity was measured using a 40 kHz ultrasonic transducer, while the terahertz radiation was measured by a silicon bolometer. Terahertz of reasonable power was detected and characterized using this method. Both the terahertz and the plasma were characterized concurrently throughout this experiment in an effort to determine the feasibility of using the ultrasonic transducer as an alignment aid. The characterization included the effects of polarization, bias, and delay on the plasma and terahertz signals. During the course of this research it was also discovered that silicon, often used as a filter to isolate the detector from the laser in terahertz research, was a significant source of terahertz as well. This experiment represents the first time THz was generated using the two color interaction modified by an external applied bias.

ACKNOWLEDGMENTS

First and foremost, I would like to thank my advisor, Lt. Col. Bohn. Without his dogged determination and insistence that "the experiment should work" I would have moved on to another, simpler, project months before I actually began to collect good data. His continual guidance and patient response to what he probably considered "silly" questions kept me moving in the right direction while giving me the freedom to make mistakes and learn valuable lessons on my own.

I would also like to thank my family for their continual support. I would like to thank them, and apologize as well, for the many hours they had to creep around the house in the evening while I studied or worked on homework. I know how difficult it can be for young boys to stay quiet and still but they did it without complaint day after day. I would also like to thank my wife for her continued encouragement, especially on those days when I was feeling inadequate or insecure. Without this constant encouragement, I would have likely given up long ago.

Finally, I would also like to thank the laboratory technicians, specifically Mike Ranft, for all the help they provided throughout the course of this research. There was hardly a day that went by during this research that I wasn't stopping by their office looking for help or asking a favor and they always came through.

Michael L. Dexter

TABLE OF CONTENTS

Page

LIST OF FIGURES

Figure Page

Figure Page

PRODUCTION AND CHARACTERIZATION OF HIGH POWER HIGH REPETITION RATE BROADBAND TERAHERTZ RADIATION IN FEMTOSECOND-LASER-INDUCED AIR PLASMA

I. INTRODUCTION

1.1 MOTIVATION

The production of high power, high repetition rate, terahertz (THz) radiation is crucial to the development of high speed THz imaging and spectroscopy systems. Until recently, the production and detection of coherent THz radiation has been both difficult and expensive. However, recent advances in continuous wave and ultrafast lasers have provided a source of THz radiation with sufficient power to be of interest in many possible applications. Yet, even with the development and widespread study of such systems, there still does not exist a tabletop model that generates enough power at a high enough repetition rate to be feasible for most imaging or spectroscopy systems. The problem lies in the fact that as the repetition rate of these systems is increased, they experience a subsequent loss in the peak pulse power. This loss in power prevents the formation of a plasma filament in air which is necessary for THz production. The applications of primary interest to this researcher are those associated with imaging, including chemical and biological weapons detection, medical and dental imaging, nondestructive testing, and security scanning.

.

Imaging with THz radiation is of significant interest because non-polarizing, non-conductive materials, including, paper, plastics, cloth, and ceramics are transparent at THz wavelengths. Since most packaging materials are comprised of these materials, THz imaging is an optimal technology for inspecting packages without compromising the integrity of the materials within. THz is non-ionizing which opens the possibility of scanning humans, whether for medical purposes, or to search for concealed hazardous items. Since many materials have distinct THz "fingerprints", including chemical and biological weapons, it is also has potential applications to both the DoD and Department of Homeland security for personnel and border security. THz imaging has also been demonstrated as an effective means for nondestructive testing on certain materials. For example, NASA is currently using a THz imaging system to search for voids and disbonds in the spray-on-foam insulation used to insulate the primary fuel tank, and is evaluating THz imaging for its potential to analyze the shuttle heat shield tiles and the ultra-high pressure gas tanks used for attitude adjustment rockets [1,2].

The system developed for this effort is designed to be used as a scanning imager, similar to a scanning electron microscope. Since each pixel in the image contains both the amplitude and phase information for each point being scanned this method of imaging provides and enormous amount of useable data. You not only capture a visible image for the object but you also capture all the spectrographic information required to determine the chemical nature of the object. However, for imaging or detection systems such as this to be commercially viable, they must be high power, have a high repetition rate, and be enclosed in a reasonably sized package.

1.2 RESEARCH FOCUS

The primary goal of this research was to attempt to fulfill the requirements of high power and high repetition rates. The high power requirement is necessary to generate a strong signal to noise ratio. Previous systems have demonstrated powers well within the requirements needed for imaging; however, most of these systems fail to meet the requirement of a high repetition rate. A high repetition rate is desirable because it generates more pulses per pixel and allows for a much faster, higher quality scan. For example, most designs to date have repetition rates ranging from 1 to 1000 Hz [3,5,6,7,8,9,10]. At 1 Hz, a standard scan of 800 X 600 pixels would take approximately 541 days, whereas a 1 kHz system, though better would still require a scan time of approximately 5.4 days to produce an image. This scan time is reduced to a more reasonable 20 minutes at 40 kHz, the repetition rate used for this research, and 0.5 seconds at 100 MHz, the repetition rate which would likely be used in a commercial system.

These goals were accomplished using a laser system with a much higher repetition rate but lower peak pulse power. The lower peak pulse power is detrimental due to the fact that a high peak power is normally required to generate the air plasma of a reasonable size. This handicap is overcome by focusing the beam to a much smaller spot size than previous attempts by other researchers. The reduction in the spot size increases the photon density such that the production of an air plasma is still viable. However, this plasma is quite weak compared to previous projects. In an effort to compensate for a much weaker plasma, a electrical bias of up to 27 kV/cm was applied across two copper electrodes. This technique has been shown to increase the THz signal generated by an air

plasma by a factor of at least 32 [3]. This amplification effect provided a strong signal which was used to optimize the setup such that a signal of reasonable power was achieved even without the bias voltage. In addition to the inclusion of the bias on the plasma, the basic experimental setup used by many other groups had to be altered. This change is due to the fact that there was physically not enough space to produce the plasma using the standard setup where the same optic is used to focus the beam on the nonlinear crystal and to form the plasma. In this experiment, three optics were used instead; one to focus the beam on the nonlinear crystal, one to collimate the beam, and one to focus the beam to form a plasma. However, the addition of a collimating optic after the nonlinear crystal introduced a delay in the blue component of the pulse when compared to the red. Therefore a delay stage had to be included to realign both pulses in time, a basic requisite for the production of THz.

1.3 BACKGROUND

The THz portion of the electromagnetic spectrum is generally quoted as ranging from 0.1 THz to 30 THz (10 to 3000 μm) as seen in figure 1. These frequencies are situated at the transition between the microwave and the infrared region of the electromagnetic spectrum. This region is a "gap" between carrier transport based electronic devices and quantum transition-based photonic devices. As a result, THz radiation has historically been difficult and expensive to produce or detect. However, because of the location of THz in the electromagnetic spectrum, it shares many favorable characteristics of both electronic and optical radiation. In electronics, electromagnetic radiation is viewed primarily as waves, wherein the electric field can be measured

directly, but is difficult to manipulate and requires bulky waveguides. However, in optics, radiation is viewed as light which can be easily manipulated with mirrors and lenses, yet the downside is that only the square of the electric field is measureable. THz can be viewed as a transition between these two regions. Like light, it can be easily manipulated with lenses and mirrors which makes it useful in the field of imaging. As with electronics, it is also possible to measure the phase allowing for spectrographic analysis to determine the chemical makeup of the object with which it interacts.

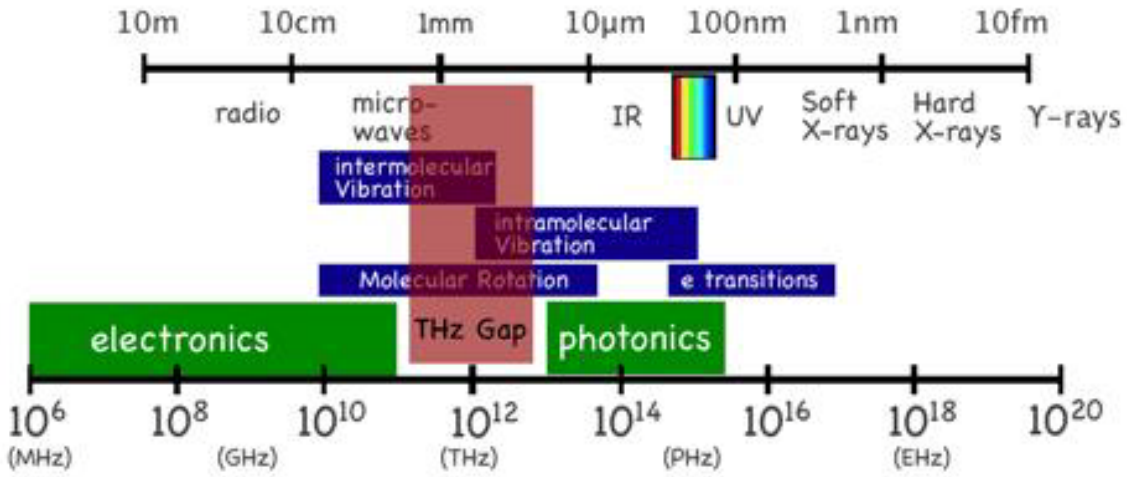

Figure 1. The electromagnetic spectrum [4].

The production of THz radiation using a laser system to generate an air plasma was first demonstrated in 1993. The signals generated using this method propagated transverse to the direction of the incident laser beam and were of very low power [5]. It was later shown that the power could be increased by applying a bias across the plasma. However, the signal generated was still of very low power and had limited uses [6].

In 2000 Cook and Hochstrasser demonstrated a system that produced THz with powers orders of magnitude higher than the previous attempts by mixing the fundamental laser wavelength at 800 nm with its second harmonic through second harmonic generation (SHG). This method generated high power THz which propagated in the direction of the laser itself as opposed to the transverse direction. Cook and Hochstrasser proposed four wave mixing (FWM) between the fundamental and the second harmonic in the plasma as the source of the new, much stronger THz signal [7]. This explanation held until recently, when another group showed that the $\chi^{(3)}$ for the plasma was too low by a factor of four to be the source of the THz radiation [8]. Since, other groups have proposed that a nonzero transient current, caused by the offset between the fundamental and second harmonic beam, is responsible for the production of the THz [9].

The first THz imaging system was demonstrated by Hu and Nuss in 1995 [10]. These images were generated by scanning an object through the focus of the THz beam where each pulse emitted by the system represents a single pixel. Further advances have been made in the field since the initial demonstration. CCD cameras were later utilized, thus removing the need to scan an object to generate a 2-dimensional image [11]. A three dimensional imaging system was demonstrated in 1997 for terahertz computed tomography and in 1998 the first terahertz near field images were reported [12,13].

1.4 PREVIEW

Chapter two of this document will discuss some of the theory necessary to fully understand the research topic, including some basic theory on ultra-short pulse propagation, nonlinear optics, ionization of gases with lasers, and production mechanisms

for THz in an air plasma. Chapter three provides a brief overview of some of the equipment used in this research including the primary laser system, a frequency doubled optical grating (FROG), a liquid helium cooled silicon bolometer, and a high speed streak camera. Chapter four lays out the methodology used to perform each step of this research to include the initial characterization of the plasma, the characterization of the plasma and pulse overlap, the fine tuning of the pulse overlap using a third harmonic crystal, and the final characterization of the plasma and THz. Chapter five mimics chapter four in a discussion of each of the main phases of the research and provides an overview and final discussion of results of this effort.

II. THEORY

2.1 ULTRASHORT PULSE PROPAGATION

An ultra-short laser pulse can most easily be described as a group of optical cycles contained within a pulse envelope and demonstrated by Figure 2.

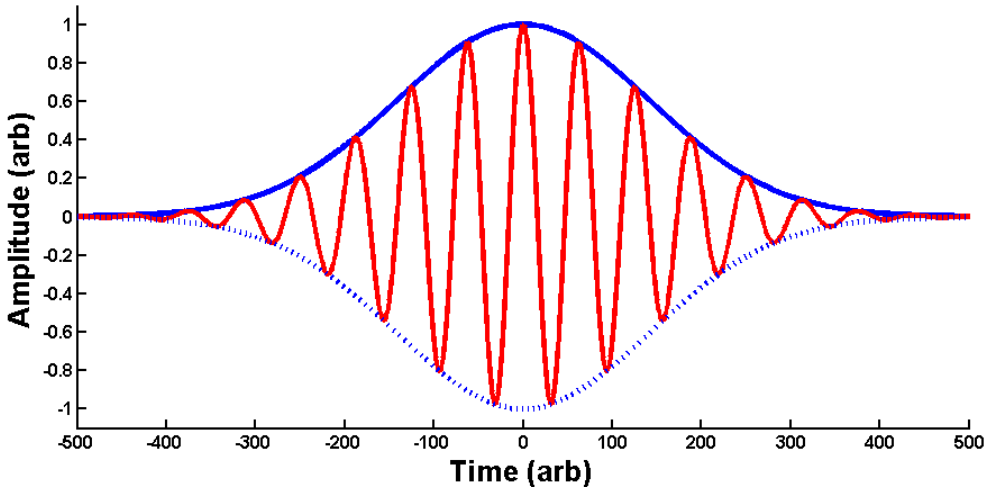

Figure 2. An example of a Gaussian pulse with no chirp

Mathematically, a Gaussian pulse is described by a collection of exponential functions, as shown in Equation (2.1).

$$\tilde{E}^{+}(t) = A_0 e^{-\omega t^2} e^{i\varphi_0} e^{i\varphi(t)} e^{i\omega_l t} \tag{2.1}$$

Where the pulse envelope is given by the real component, $A_0 e^{-i\alpha t^2}$, ω_l is the carrier frequency, φ_0 is the initial phase and $\varphi(t)$ is the phase as a function of time. The total instantaneous phase of the pulse is then given by $\varphi_0 + \varphi(t)$. Taking the first time derivative of the instantaneous phase, $\frac{d}{dt}\varphi(t)$, gives the instantaneous frequency, the rate at which the total phase propagates forward in time. This expression is referred to as the "chirp" of the pulse. An example of a chirped pulse can be seen in Figure 3. As is clear from the figure the higher frequency components of the pulse have been shifted forward

while the lower frequency components are shifted in the opposite direction. This configuration is referred to as up-chirp. A pulse can also be down chirped. In this case the process is simply the reverse of up-chirp. The sign of the second derivative $\frac{d^2}{dt^2}\varphi(t)$ of the instantaneous phase tells you whether a pulse is up-chirped or down-chirped. If the sign is positive it is up-chirped, if it is negative it is down-chirped.

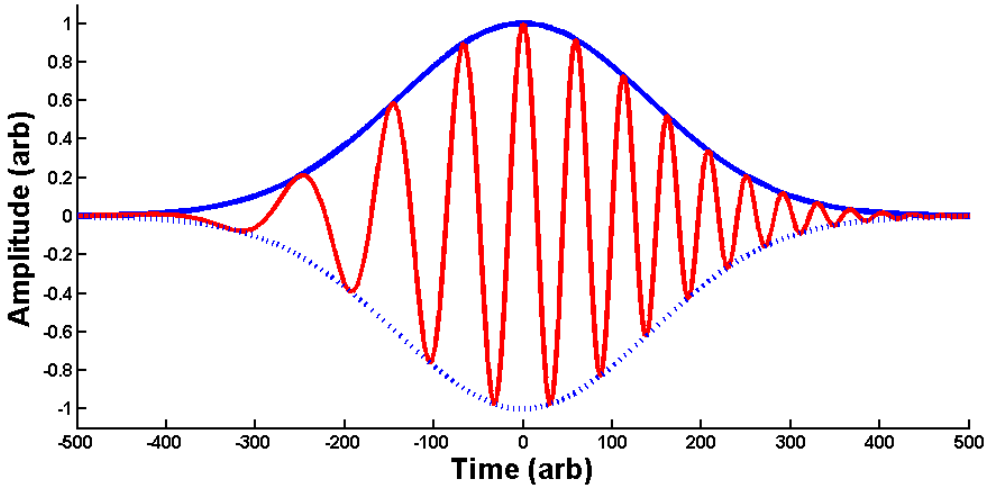

Figure 3. An example of an upchirped Gaussian pulse

Chirp is important because if a pulse is sent through a medium in which different frequencies propagate at different speeds, the chirp can either be enhanced or reduced, thus expanding or compressing the pulse [14]. For this research, the maximum amount of peak power possible is needed to achieve plasma formation. Due to this requirement, the laser pulse is up-chirped to pre-compensate for all the dispersive elements in the this system so that the minimum possible, or transform limited, pulse width is achieved at the point of plasma formation.

Another important property of ultra-short pulses is the manner in which they travel through a media. To better understand this principle a brief overview of basic

electromagnetic theory is required. Equation (2.2) defines a propagation constant k for a wave traveling in a medium,

$$k = \frac{2\pi v}{c} n(\lambda) \tag{2.2}$$

where c is speed of light and $n(\lambda)$ is the index refraction as a function of wavelength. The group of optical cycles contained by the pulse envelope travel at the phase velocity, while envelope itself travels at the group velocity. The phase velocity is given by $v_p = \frac{c}{n(\lambda)}$, and the group velocity is defined in Equation (2.3).

$$\frac{1}{v_g} = \frac{\partial k}{\partial \omega} = \frac{n}{c} - \frac{\lambda}{c}\frac{dn}{d\lambda} \tag{2.3}$$

It can be clearly seen in Equation (2.2) that the group velocity is frequency dependent. Therefore, as the pulse travels through a dispersive media, either the higher (blue) frequencies will pull ahead of the lower (red) frequencies, or the red will "catch up" depending on the dispersive properties of the medium. This behavior is known as Group Velocity Dispersion (GVD). GVD is given by the derivative of the group velocity defined by Equation (2.4).

$$k'' = \frac{d^2k}{d\omega^2} = \frac{\lambda^3}{2\pi c^2}\frac{d^2n}{d\lambda^2} \tag{2.4}$$

Whether a material has positive dispersion or negative dispersion is based on the sign of k". For an upchirped pulse, positive GVD stretches the pulse in time, while negative GVD compresses the pulse. The GVD is important in this experiment due to the fact that after the formation of the blue pulse in the nonlinear crystal, both the red and blue components of this pulse must travel through media with positive GVD. This translation through a dispersive media causes the blue component of the pulse to lag

behind the red. To compensate for this effect, the red and blue components of the beam were split using a beam splitting optic and a delay stage was introduced on the red side so that the blue component could "catch up". This delay was adjusted such that the red and blue components, when recombined, overlapped once again in both space and time, a requirement for the generation of THz using this method. Using Equation (2.3), along with the appropriate Sellmeier coefficients, it is possible to calculate the delay induced between the two pulses by the collimating lens. Calculations show, that for the lens in this system, a delay of approximately 790 fs, or 0.236 mm is present. This delay may seem insignificant, yet results from this experiment show that the pulses must be within 13 femtoseconds of each other to effectively generate THz without an added bias.

2.3 Nonlinear Optics and Third Harmonic Generation

To discuss the properties of nonlinear optics we must first start by looking at the wave equation of the electric field shown in Equation 2.4.

$$\nabla^2 E = \frac{1}{c^2}\frac{\partial^2 E}{\partial t^2} = \frac{1}{\varepsilon_0 c^2}\frac{\partial^2 P}{\partial t^2} \tag{2.4}$$

From which the polarization density P can then be expressed as a Taylor series in the applied field,

$$\mathrm{P} = \varepsilon_0(\chi_1 E + \chi_2 E^2 + \chi_3 E^3 + \ldots) \tag{2.5}$$

where χ_1, χ_2 & χ_3 are the linear, second-order and third-order optical susceptibilities of the medium [15]. As seen in Equation (2.4), the polarization affects the propagation of

the electric field through a medium while Equation (2.5) shows that the higher order terms become more important as you increase the field strength. For relatively weak electric fields, the polarization is linear and the response of the medium is simply given by the index of refraction. However, for stronger fields, the second and third order terms begin to affect the response of the medium. Second-order nonlinearity produces effects including frequency doubling or second-harmonic generation (SHG), sum and difference-frequency generation, and parametric amplification and oscillation [15]. The third-order nonlinearity drives effects, including Self-Phase Modulation (SPM), the optical Kerr effect, Raman scattering, third-harmonic generation, and four wave mixing.

Of these many nonlinear effects, the two most important to this work are second harmonic generation and four wave mixing. Second harmonic generation, otherwise known as frequency doubling or sum frequency generation, is a χ_2 effect in which you take two photons and add them together to get a third photon with a frequency equal to the sum of the frequency of the original two and an equivalent bandwidth. Second harmonic generation is used in this experiment to generate the a secondary beam at 400 nm and sum frequency generation is used to generate 266 nm light as a diagnostic tool to determine the accuracy of the pulse overlap. The 400 nm beam is generated by focusing the 800 nm fundamental beam onto a specially fabricated Beta-Barium Borate (BBO) crystal. This 400 nm (second harmonic) beam is generated collinear with a perpendicular polarization to the fundamental beam.

A similar process is used as a diagnostic tool to determine the pulse overlap. After rotating the 800 nm beams polarization with a half wave plate at 800 nm, and passing it through a delay stage to compensate for dispersion, the 800 nm and 400 nm

beams are recombined and then focused onto a second BBO crystal where sum frequency mixing occurs and a third frequency at 266 nm is produced. This process only occurs when both the red and blue pulses are overlapped in both space and time. The requirements for this nonlinear effect to occur are far less exacting than those for THz production, therefore this method provides a means of adjusting the system in a regime in which it is not possible to actually generate THz.

In practice, four wave mixing is very similar to second harmonic generation. However, four wave mixing is a $\chi^{(3)}$ effect. It can be most easily explained by the simple addition or subtraction of photon frequencies. You simply take 3 photons and add or subtract them in such a way as to generate a fourth photon equal to the sum and/or difference of the frequencies of the three but again with an equivalent bandwidth. A few examples of four wave mixing are shown below.

$$\omega_4 = \omega_1 + \omega_1 + \omega_1 = 3\omega_1 \tag{2.5}$$

$$\omega_4 = \omega_1 + \omega_2 - \omega_3 \tag{2.6}$$

$$\omega_4 = \omega_1 + \omega_2 + \omega_3 \tag{2.7}$$

Four wave mixing is important to this work because it was used as the standard explanation as the production mechanism for THz in a plasma until recently. This method of production is describe by Equation 2.8 below.

$$\omega_{\mathrm{BLUE}} - 2\omega_{IR} = \omega_{THz} \tag{2.8}$$

However, recent research has shown that the value of $\chi^{(3)}$ for a plasma is much too small for this process to occur [16]. Fortunately, a new theory has been proposed to explain the mechanisms responsible for THz production in air plasma as a result of

mixing the fundamental and second harmonic. This theory will be discussed in more detail later in this paper.

2.4 Ionization of Air With a Laser

The ionization of a gas, specifically N_2, is the means in which the plasma is generated in this experiment. However, the creation of a plasma in air is not quite as straightforward as it may seem. Under normal intensities, the only mechanism for the ionization of an atom using photons is the photoelectric effect. The photoelectric effect requires that an atom absorb energy in discrete quanta equal to the ionization potential of that atom or $h\upsilon$. For N_2 this ionization potential is 15.58 ev [17]. However, the ionization energy of the laser used in this experiment is only 3.10 ev at 400 nm and 1.55 ev at 800 nm. So according to basic photoelectric theory, this laser system should not be capable of ionizing air. However, additional effects come into play when dealing with extremely high photon densities and electric field intensities available with ultra short pulsed laser systems.

There are two primary mechanisms for the ionization of atoms in an ultra short pulsed laser system; multiphoton ionization and tunneling/above threshold ionization. Multiphoton ionization, as its name implies, is an effect which utilizes several photons to provide the necessary energy to free an electron. The likelihood of this process occurring is strongly dependent on the photon density. According to perturbation theory, the n-photon ionization rate is given by Equation 2.10

$$\Gamma_n = \sigma_n I_L^n \tag{2.9}$$

where σ_n represents the cross section for the event to occur which decreases with n while I_L^n is the laser intensity which at high enough intensities can overcome the decrease in cross section [18]. For multiphoton ionization to occur laser intensities greater than 10^{10} Wcm^{-2} are required. These laser intensities are easily achievable in commercially available systems. For example the system used in this research produces an intensity at the focus of over $2.5x10^{14}$ Wcm^{-2}.

The second mechanism capable of ionizing a gas using coherent light is tunneling/over the barrier ionization. The effect is described as tunneling/over the barrier ionization due to the fact that they are essentially the same mechanism occurring at different external electric field strengths. Tunneling ionization is an effect that occurs when the field strength of the laser approaches the atomic field strength given by Equation 2.10.

$$E_a = \frac{e}{4\pi\varepsilon_0 a_B^2} \simeq 5.1 \times 10^9 \ Vm^{-1} \tag{2.10}$$

This relationship can be converted to a laser intensity vs. atomic intensity by the relation in equation 2.11.

$$I_a = \frac{\varepsilon_0 c E_a^2}{2} \simeq 3.51 \times 10^{16} \ Wcm^{-2} \tag{2.11}$$

Tunneling ionization occurs as a result of the suppression Coulomb potential by an external electric field (laser field). This suppression creates a regime in which quantum mechanical electron tunneling may occur. The closer the electric field is to the atomic field strength, the higher the probability the electron will tunnel and be liberated. When this field exceeds the atomic electric field, the barrier is suppressed to such a degree that

tunneling is no longer necessary and the electron is simply spontaneously emitted. This effect is referred to as the previously mentioned over the barrier ionization [18].

The relationship between the laser frequency the ionic field strength, and the laser intensity determine whether an electron is liberated by a multiphoton process, or a tunneling process. This relationship is quantified by the Keldysh parameter defined by Equation 2.12.

$$\gamma = \omega_L \sqrt{\frac{2E_{ion}}{I_L}} \backsim \sqrt{\frac{E_{ion}}{\Phi_{pond}}} \tag{2.12}$$

where

$$\Phi_{pond} = \frac{e^2 E_L^2}{4m\omega_L^2} \tag{2.13}$$

is the ponderomotive potential of the laser field. As a general rule of thumb, if the Keldysh parameter is less than one then multiphoton ionization is the dominating ionization mechanism, if it is greater than one then tunneling ionization is responsible. If the value is near one then you can assume that both processes are taking place with neither dominating. However, it should be noted that these relationships begin to break down a bit for large many-electron atoms [18]. For the system used in this work, the Keldysh parameter is 0.65 which puts it in the regime of multiphoton ionization, but since it is not significantly less than one you can assume that tunneling is also likely.

2.5 Terahertz Production in Air Plasma

The mechanisms for the production of THz in an air plasma are many, varied and still under debate at the time of this writing. The theories describing each mechanism vary significantly depending on the experimental setup.

For the simplest case, an experiment using a single wavelength, notably 800 nm, two mechanisms for the production of THz have been proposed. The first states the THz generated is the result of radiation pressure induced by the laser pulse which causes longitudinal plasma oscillations with a frequency equal to the plasma frequency [19]. For an electron density consistent with these experiments, $n_e = 10^{16} cm^{-3}$ and the plasma frequency is given by Equation 14 as

$$\omega_{pe} = \sqrt{\frac{n_e e^2}{m_e e_0}} \approx 6 \text{ x } 10^{12} \text{ rad s}^{-1} \tag{2.14}$$

The second theory states that THz is generated by the ponderomotive force. In essence, the ponderomotive force results from a transverse intensity gradient in the spatial dimension of a laser beam with a Gaussian profile. This gradient causes the electrons in the beam to preferentially move away from the higher intensity central region to the lower intensity outer region. This resulting flow of electrons sets up a transverse current which is responsible for the production of the THz pulse [20].

This theory becomes more complicated when an electrical bias is applied across the plasma filament as done in several of the experiments performed during the course of this research. Not only do you have to account for the two previously mentioned effects, but another becomes important at high static field strengths. This effect is the result of the longitudinal oscillations of the plasma left in the wake of a moving ionization front generated by the laser pulse. These oscillations are excited by the ponderomotive force and heavily damped by electron collisions on a picosecond time scale. They are greatly enhanced by a static electric field which produces a strong THz pulse. This radiation is

emitted by a dipole like structure moving at the speed of light and is similar to a Cherenkov emission created by a pair of opposite charges. The THz emitted by this configuration propagates in a narrow cone along the direction of the beam [21].

Another level of complexity, and even controversy, is added when you begin to mix the fundamental at 800 nm with its second harmonic at 400 nm. As mentioned previously in this paper, the first group to generate THz using this technique was Cook and Hochstrasser in 2000. They concluded that the THz generated by this method was the result of four wave mixing. However, it was recently shown by another group that that the $\chi^{(3)}$ for plasma is too low by a factor of four [8]. The most accepted theory to date was proposed by a group in 2007. In their most recent paper they summarize the process as follows:

> In this (plasma current) model, bound electrons of gas-phase atoms or molecules undergo rapid tunnel ionization as the Coulomb barrier is suppressed by the instantaneous laser field. Owing to its highly nonlinear and phase-sensitive nature, the ionization occurs mostly at the peaks of the combined two-colour laser field, which can be different from the peaks of the individual fields. Electrons arising in such an asymmetric laser field can acquire a nonzero drift velocity, producing a direction electron current with simultaneous emission of THz radiation in the far-field. Quantum mechanically, this asymmetric current occurs due to the interference between two ionization pathways (single-photon and two-photon), which excite bound electrons from an initial discrete state to a final continuum state [22].

In essence, they claim that the source of the THz in this configuration is the result of a nonzero transient current, caused by the offset between the fundamental and second harmonic beam. They showed that a non-zero electron drift velocity

$$v_d = \frac{eE_1 \sin\phi}{m_e\omega} + \frac{eE_2 \sin 2\phi + \theta}{2m_e\omega} \tag{2.14}$$

is present for electrons born at ϕ laser phase when the relative phase θ between the fundamental frequency ω and 2ω is equal to $\pi/2$. This drift velocity leads to a transverse electron current $J_{\perp}(t) = \int_{t0}^{t} e v_e(t,t') N_e(t') dt'$ which then produces the observed THz pulse [9].

III. EQUIPMENT

3.1 VERDI-PUMPED FEMTOSECOND LASER SYSTEM

The laser used in this research is a Coherent fs pulsed laser system as shown schematically in figure 4. The 18 W Verdi beam pumps the 76 MHz MIRA, which produces 50 fs pulses at a central wavelength of 800 nm. The pulses then undergo Chirped Pulse Amplification, beginning with the expansion module. Each pulse is stretched out in duration to approximately 200 ps, which greatly reduces the peak power. The pulse is then directed into the RegA (also pumped by the Verdi), where it is amplified in approximately 20 round trips. While the RegA is tunable anywhere between 10 and 300 kHz, this research was conducted at 40 kHz in order to optimize the detection of the plasma using the 40 KHz resonant ultrasound detector. The pulse is then re-compressed, resulting in a beam comprised of 50 fs pulses at the repetition rate of the RegA, with a central wavelength of 800 nm, a beam diameter of 2.68±.02 mm, and a typical average power of 350 mW. The pulse peak energy is then approximately .350 W/40 kHz, or about 8.75 μJ. While each 8.75 μJ pulse is of fairly low energy, the peak power of the laser is quite high: $8.75\mu J/50fs = 1.75 * 10^8/W$. The first turning mirror (after the compressor) has a reflectivity of 99.9%, which provides a diagnostic beam of .1% of the system's output for beam characterization equipment such as a Grenouille [23].

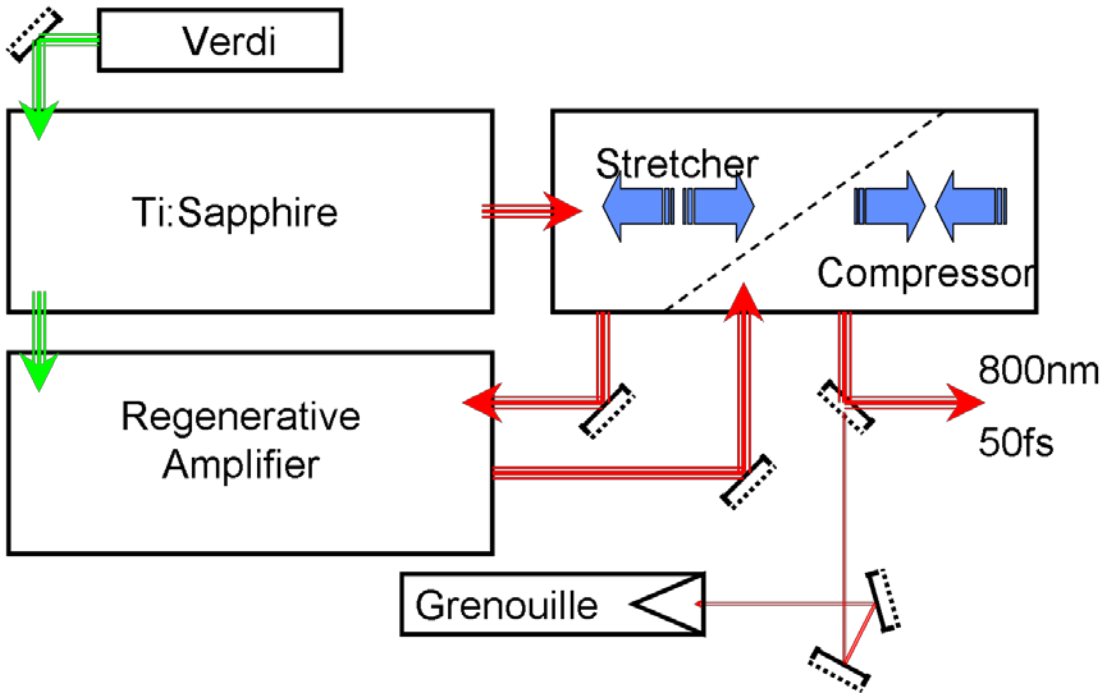

Figure 4. Schematic of Coherent fs-pulsed laser system with Grenouille

3.2 Frequency-Resolved Optical Grating (FROG)

Due to the extremely short timescales which these laser pulses exist, it is not possible to measure their characteristics directly. However, methods have been developed that allow for some information to be obtained about them. For instance, autocorrelation allows you to measure the pulse width of an ultrashort pulse by interfering the pulse with itself using a nonlinear crystal coupled with an interferometer. Unfortunately, a drawback of this system is that you must use the pulse to measure the pulse, which results in a loss of pulse structure due to averaging effects inherent in the calculations, and it provides no information on the phase or chirp of the pulse. An improvement to method was presented by Kane and Trebino in 1993 known as frequency

resolved optical gating or FROG [24]. The basic design of a second harmonic generation (SHG) FROG is shown in Figure 5.

The Grenouille is a simplified version of an SHG FROG. It uses a thick SHG crystal and various optical components to simplify the system by eliminating the need for an optical delay line. When paired with the QuickFrog software package, ultrashort laser pulses can be measured by the device and viewed in real time. The Grenouille measures both spatial and temporal parameters, using an SHG crystal and CCD camera to give instantaneous feedback on wavelength, pulse width, intensity, phase vs. time, spatial profile, spatial chirp and pulse-front tilt [23]. Like an autocorrelator, the Grenouille measures the symmetric laser pulse width in addition to the FWHM value for τ. Although it does measure spatial chirp, one drawback to the Grenouille is that is does not provide any information on the temporal chirp of the pulse. Another drawback is that the sign of the measured chirp is ambiguous.

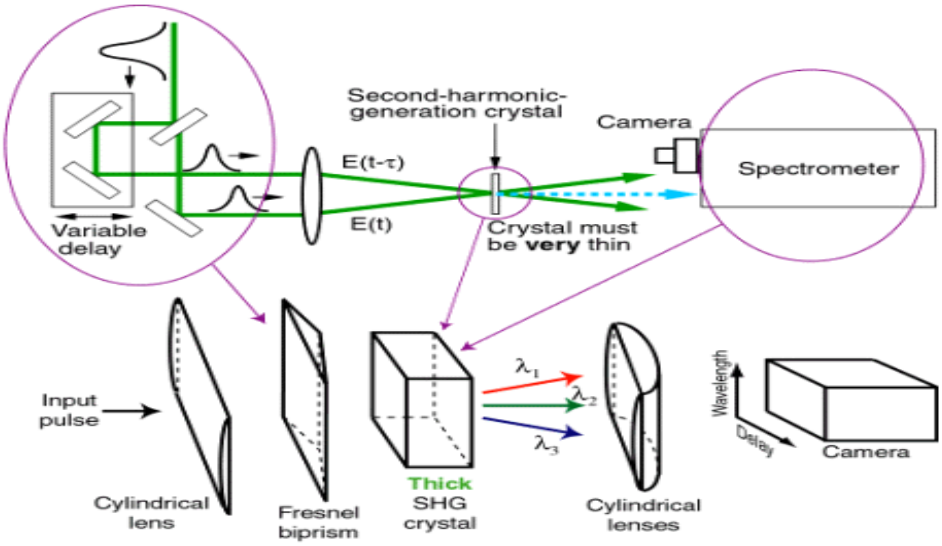

Figure 5. Typical FROG and Grenouille diagram [24].

3.3 Liquid Helium Cooled Silicon Bolometer

The primary THz detector used for this research was an IR Labs 1.6° K liquid helium cooled silicon bolometer. The detector is made up of three main parts: the detector, mounted on a silicon substrate, the liquid helium dewar, and an LN-6C preamplifier. The bolometer is mounted in a side looking configuration with a Winston cone collector, a three-position filter selector wheel, far infrared cut-on type filter and isolated by a wedged Polyethylene vacuum window with a 10-20 micron diamond powder layer. It is of the composite type, where a small silicon element is thermally bonded to a suitably blackened 3.0 mm diameter diamond absorber mounted in a cylindrical cavity. The parabolic cone has an entrance aperture of 12.7 mm at a focal ration of 3.8 and an exit aperture of 1.6 mm and is gold plated [23].

The basic system spectral response is determined by the 3 far-infrared cut-on type filters mounted on the three-position filter selection wheel. These filters include a 300 micron filter made of crystal quartz with diamond scatter layer, a 100 micron filter made of crystal quartz, 1 mm thick, over coated on one face with Garnet powder, and a 35 micron filter made of flourogold in series with black polyethylene [23].

The basic theory of operation for this type of detector is straightforward. The absorption of radiation by free carrier electrons results in a rise in their mean temperature away from and above that of the host silicon crystal lattice. The mobility of the electrons, μ, is a function of temperature which is given by $\mu = CT^{3/2}$ where C is a constant. The change in electron mobility is detectable as a change in the impedance of the crystal. This change in impedance is then amplified by the preamplifier and the signal is measured by external instrumentation, for this research, a lock in amplifier [26].

3.4 HAMAMATSU STREAK CAMERA

A Hamamatsu model C6860 streak camera was used to characterize the plasma and "dial-in" the pulse overlap. The camera operates at a frequency of 76 MHz, has a spectral response ranging from 200-850 nm, and has a time resolution as low as 45 ps.

The heart of the streak camera is the streak tube. The streak tube is very similar to a tube television set. Incoming light impinges on a photocathode, converting the light into a number of electrons which are proportional to the incident light intensity. These electrons are then directed through the tube by accelerating electrodes. The electrons pass between a pair of parallel deflection plates where a high voltage is swept in sync with the laser repetition rate. This sweeping voltage displaces the electrons horizontally by varying amounts depending on their time of arrival as compared to the frequency of the sweep voltage. These electrons are then multiplied by a micro-channel plate. These electrons then impinge on a phosphor screen which converts their energy into a visible image on the screen. This image is detected by a charge coupled device (CCD) and displayed and analyzed using the streak camera software [27].

IV. METHODOLOGY

4.1 EXPERIMENTAL OVERVIEW

Nearly all experiments performed during the course of this research share similar characteristics in the basic setup. Normally, the only change made to this setup was a change of detectors. However, the methodology and purpose of each experiment varied significantly, therefore, each phase of the research is discussed independently.

The core setup for this research is shown in Figure 6. The input beam exits the laser and is reflected off a 99.9% mirror. Thus, 0.1 % of the incoming light is directed into the FROG for laser characterization. The other 99.9% is directed onto a lens which focuses the beam onto a BBO crystal where the second harmonic is generated at 400 nm. These two beams then propagate to a second lens where they are collimated.

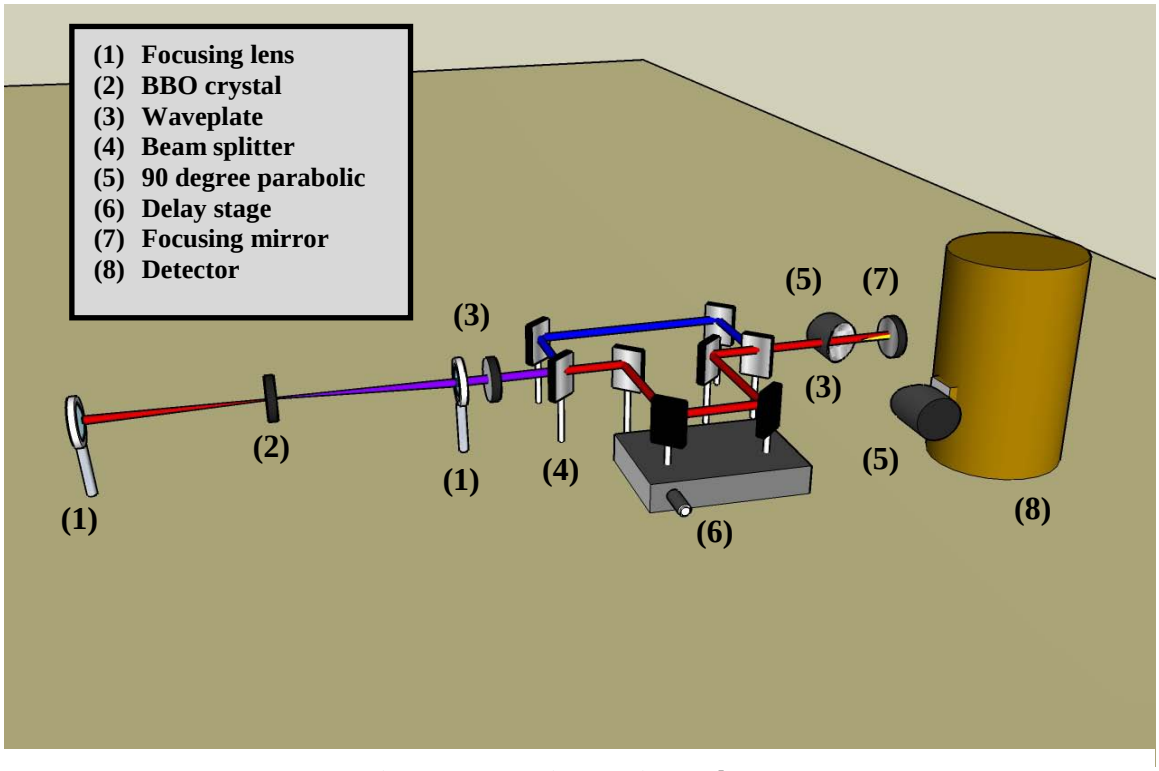

Figure 6. Generic experimental setup

The beam then impinges on a beam splitter which separates the red and blue components by passing the red and reflecting the blue. The blue component is reflected by the beam splitter and is directed by two mirrors back to a second beam splitter where it is recombined with the red. The red component then passes through a half wave plate to realign the polarization to match the blue. It is then reflected by a mirror to a delay stage and then is reflected by another mirror and recombined in the second beam splitter with the blue component. The newly adjusted and combined beam is then directed onto a 3.75 cm focusing mirror which focuses the beam to spot size of approximately 2.7 microns to generate a plasma.

The plasma is generated slightly off axis between two copper electrodes, which can be used to apply a bias of up to 27 kV/cm, and at the focus of a 90 degree off axis parabolic mirror with a 5.08 cm focal length. This mirror collimates the signal which is then collected by a second parabolic mirror, with a focal length of 11.5 cm, which reimages the signal into the detector of choice.

4.2 Characterization of Plasma and Pulse Overlap

The primary objectives for this experiment were to dial in the pulse overlap, which is necessary for a detectable THz signal, and characterize the plasma decay. These objectives were accomplished using the Hamamatsu streak camera. The setup for this experiment was very similar to that shown in Figure 6 with the exception that a cylindrical planar convex lens was placed between the focusing parabolic and the

detector. Also, during the measurement of the plasma lifetime, a filter with a band pass at the nitrogen emission line at 337 nm was used to isolate the camera from the laser.

Due to the fact that the time parameters of the camera change based on the sensitivity of the time axis, the system was calibrated using a 400 ps Fabry Perot optic. The optic was placed in the cavity with only the blue component of the input beam present. With the optic in the cavity, a series of interference fringes, each spaced approximately 400 ps apart was detected by the camera. This image was then used to qualify later images by providing a time/pixel on each image. The data collected for these measurements can be seen in Figure 7. Figure 8 is a graphical representation of this data. As can be clearly seen, there exists a periodic series of maximums corresponding to the delay of the Fabry Perot optic. However, it is clear that these peaks are not equally spaced. This is likely due to the difference in the path lengths for the light that comprises each subsequent peak. This increase in path length will systematically increase the delay between each successive peak. For that reason, only the peak to peak value between the first and second peaks were used to determine the calibration constant for the subsequent datasets. As can be seen in figure 8, the delay between the first and second peak is 204 pixels which gives a time/pixel value of 1.96 ps/pixel.

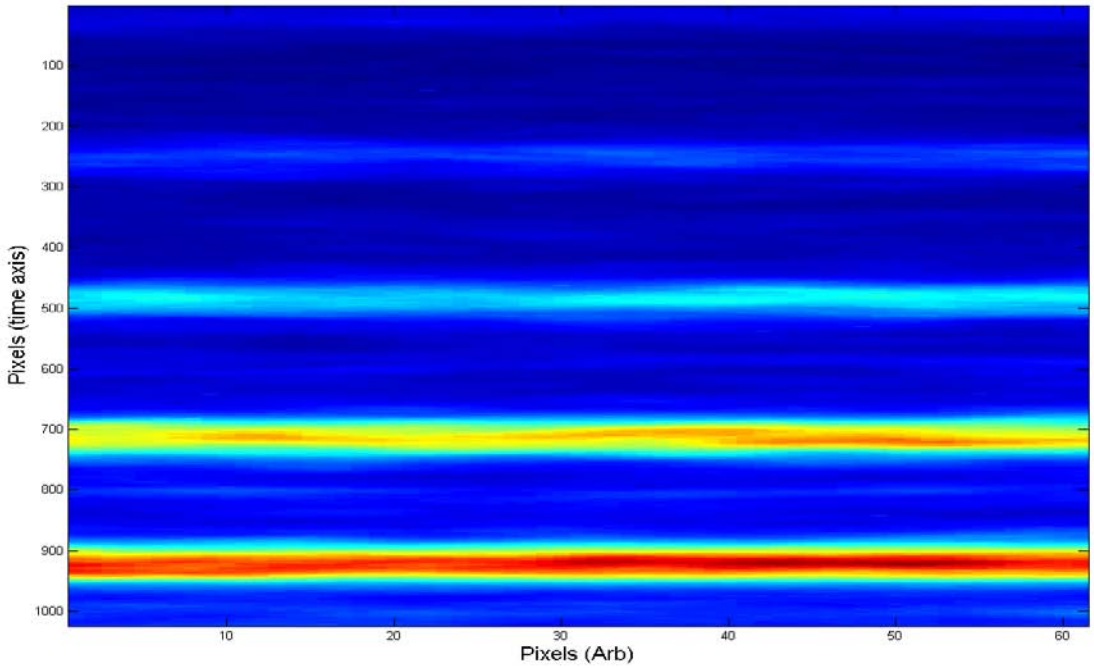

Figure 7. Raw data used to calibrate the time axis of the streak camera

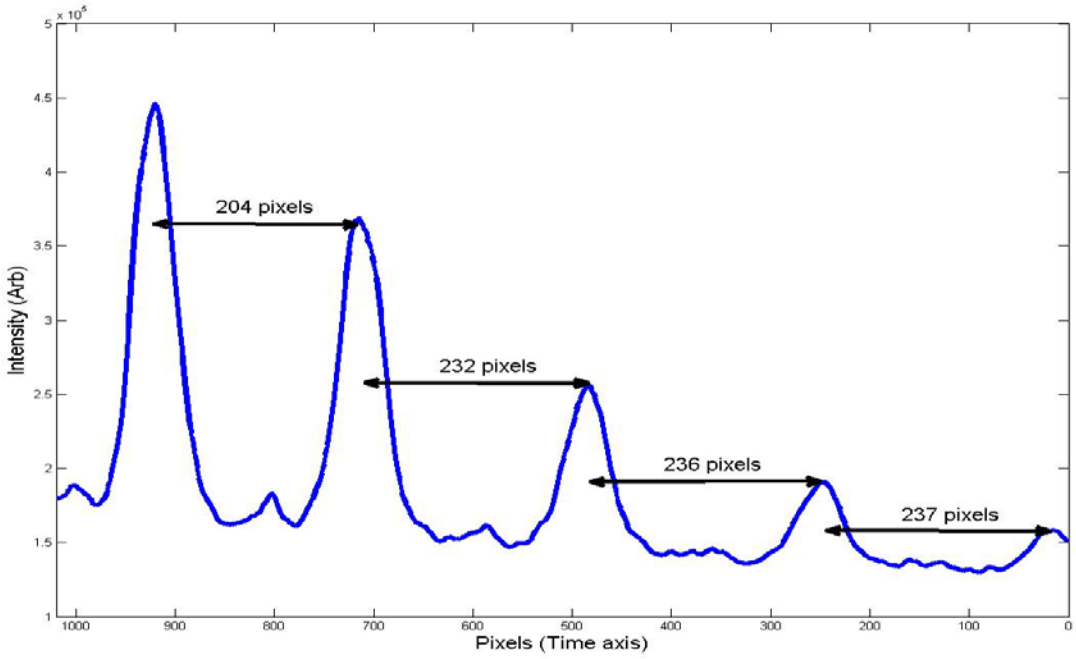

Figure 8. Processed data used to calibrate the time axis of the streak camera

The first goal of this experiment was to measure the delay in the red and blue pulses and adjust the delay stage such that the two pulses overlapped. The position of the mirrors on the delay stage was measured such that the delay between the two pulses was spatially accurate to within a centimeter. However, for the production of THz this delay needed to be on the order of a few microns. Due to the many degrees of freedom associated with setup, it was decided that the pulse overlap should be determined in a stepwise approach. Since the streak camera has a time resolution on the order of 50 picoseconds, it was possible to measure the pulse overlap to within 0.05 millimeters, approximately two orders of magnitude more accurate than measuring by hand.

The technique used to measure the pulse overlap was fairly straightforward. A small piece of diffuse material was placed at the focus of the beam. This material was illuminated by beam and produced a reasonably bright source of secondary illumination due to the interaction of the laser with the material. Since the laser beam actually consisted of two independent strings of ultra short pulses, one set delayed when compared to the other, each pulse illuminated the material at a different point in time. This illumination was collimated by the collecting parabolic and refocused onto the cylindrical lens by the focusing parabolic. A cylindrical lens was used to produce an image which was uniform along the time axis to permit easy measurement of the signal.

Examples of the data collected for this experiment are show below in figures 9-12. Figure 9 shows an image taken when the two pulses were not overlapped. As you can see the blue component is significantly brighter than the red component due to the fact that the camera is more sensitive to this portion of the spectrum. As can be seen in both figures 9 and 10 the delay between the red component and the blue component is

approximately 422 picoseconds. This translates to approximately 127 mm of delay between the two pulses. Figures 11 and 12 show the image and plot respectively, after the pulses were aligned with the delay stage.

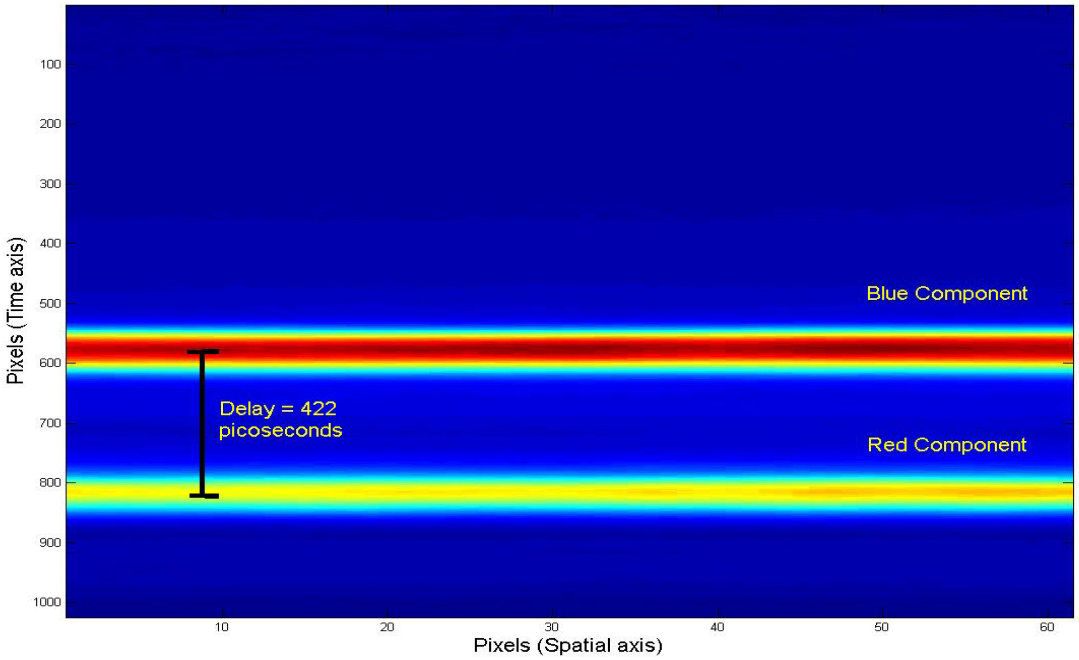

Figure 9. Image of the red and blue pulses as they appear when not overlapped

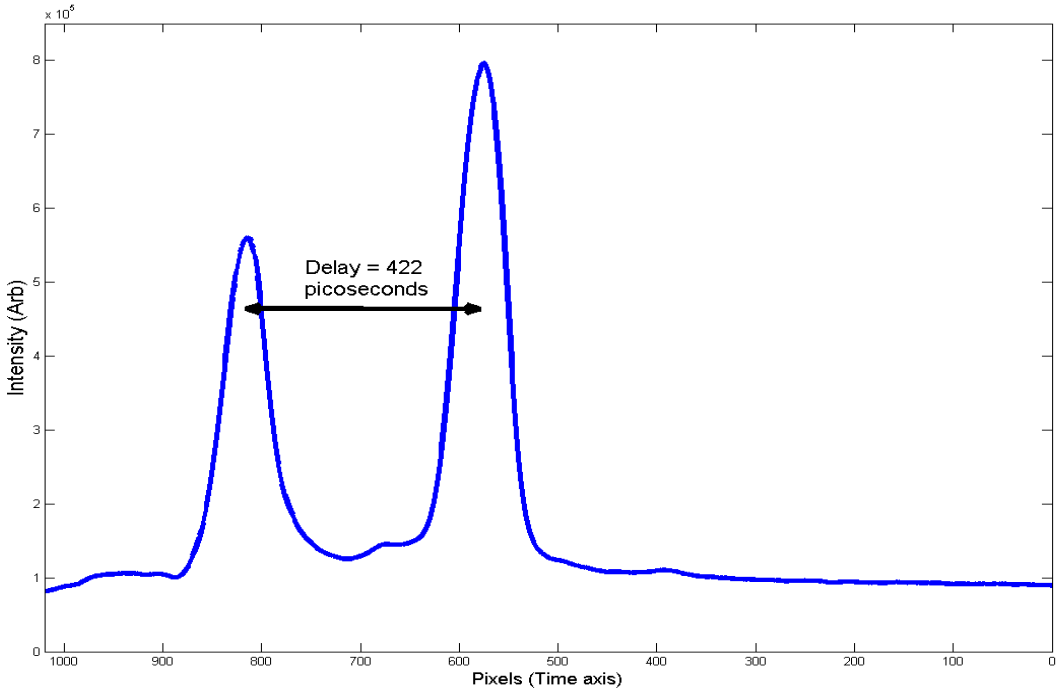

Figure 10. Plot of the red and blue pulses as they appear when not overlapped

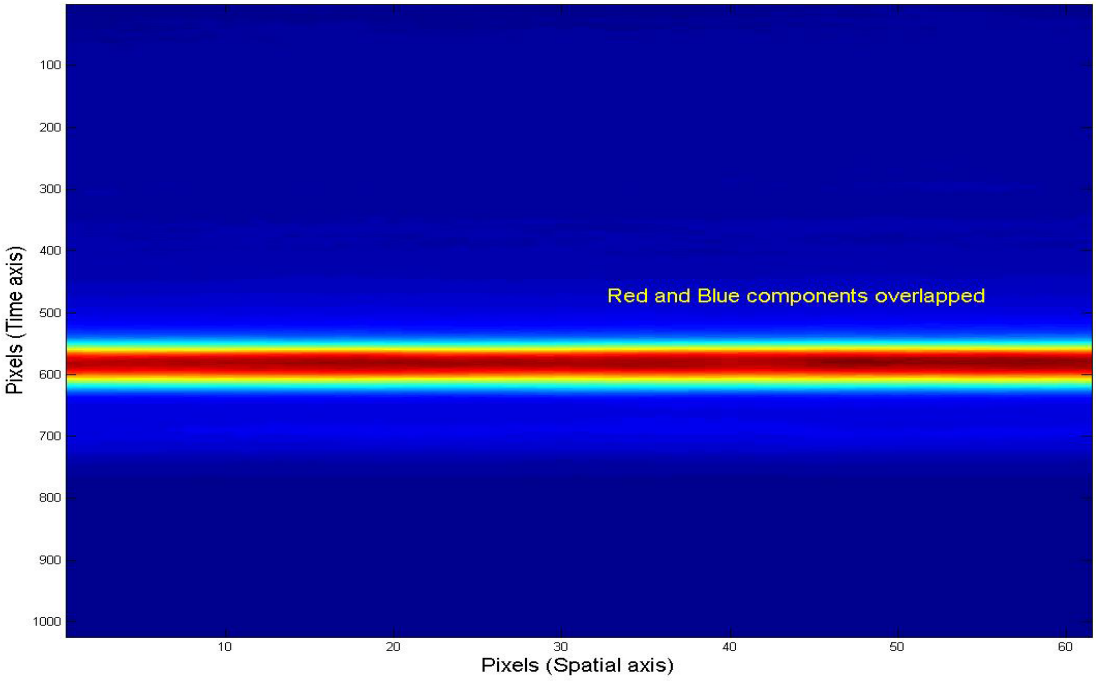

Figure 11. Image of the red and blue pulses as they appear when overlapped

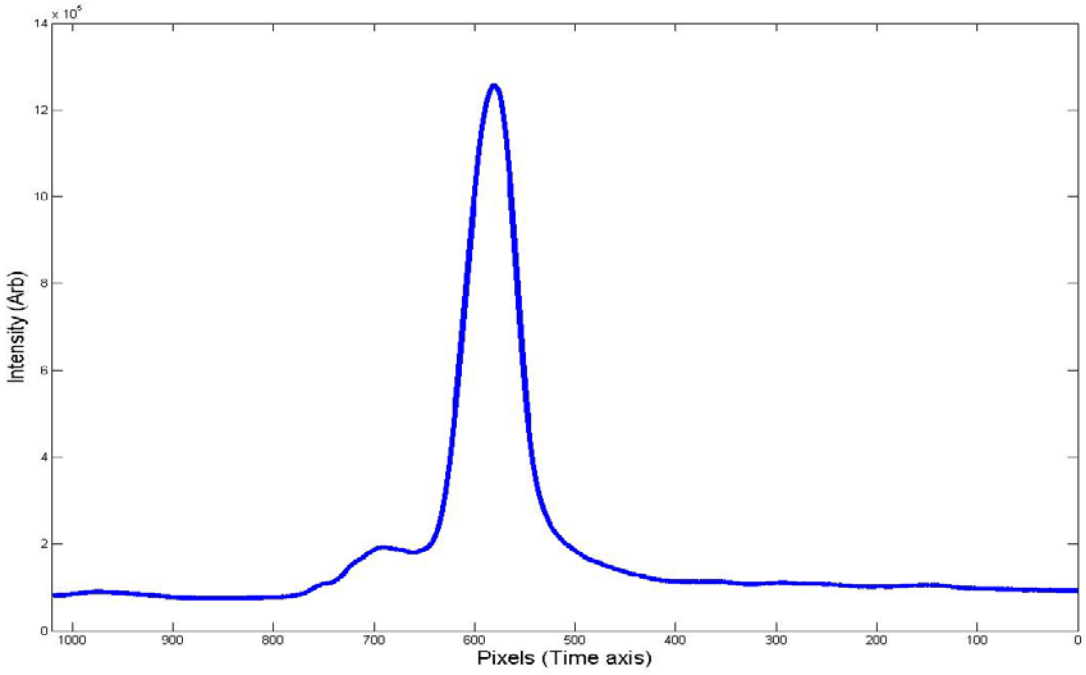

Figure 12. Plot of the red and blue pulses as they appear when overlapped

In addition to determining the pulse overlap, the plasma lifetime was also measured using the streak camera. The setup for measuring the plasma lifetime was nearly identical to that used for measuring the pulse overlap, with the exception at the diffuse material was removed from the focus so that the plasma itself could be imaged. A filter designed to only pass 337 nm light was also placed in front of the camera in order to isolate the nitrogen emission line at this wavelength. Since the brightness of the plasma was orders of magnitude dimmer than the diffuse material used in the previous experiment, the integration time required to image it was significantly longer and several images were collected and averaged to provide the clearest possible signal. An automated background subtraction was also performed on each image to eliminate background noise cause by damaged pixels.

4.3 Fine Tuning Pulse Overlap Using Third Harmonic Crystal

The work accomplished with the streak camera allowed the pulse overlap to be determined to within approximately 15 mm. However, as mentioned before, to generate THz, the pulse overlap needed to be within a few microns. The next step in accomplishing this goal was to use sum frequency mixing in a BBO crystal to generate the third harmonic at 266 nm. The requirements for the generation of this third harmonic are nearly as stringent as those required to produce THz. However, as discovered during these experiments, the conditions for good pulse overlap in the crystal are not the same as the conditions in the plasma. The differences in the physical size and composition of the crystal when compared to the plasma slightly alter the position of pulse overlap. In addition, the range in which the pulse overlap was satisfactory in the crystal was approximately an order of magnitude higher than in the plasma. However, even with these limitations, this method provided a means of adjusting the alignment of the system to such a degree that finding the pulse overlap in the plasma required only a minor adjustment to the delay.

The setup for this experiment is similar to that shown in Figure 6, with a few additions which are detailed in Figure 13. For these measurements, a 90 degree parabolic mirror was placed in the beam path between the second beam splitter and the collecting parabolic. The beam was focused onto a BBO crystal to generate the third harmonic. The resulting beam, now comprised of a fundamental, second harmonic, and third harmonic, impinged on a mirror designed to pass the fundamental and second harmonic while passing the third harmonic. This third harmonic beam was then directed onto a diffuse surface where it was detected using an Ocean Optics spectrometer.

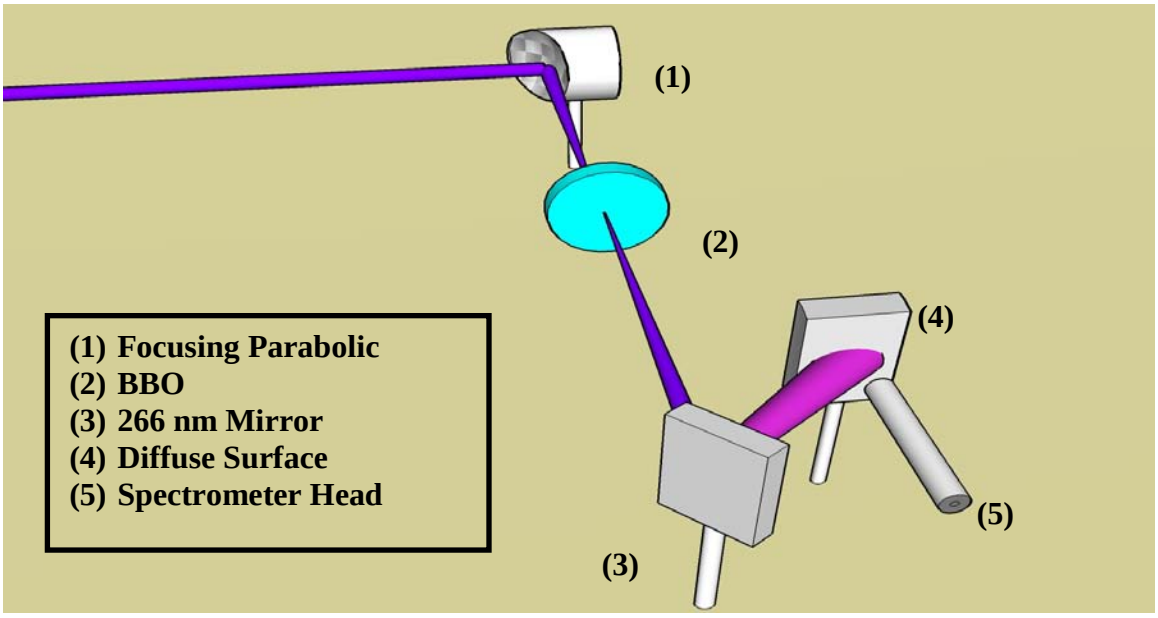

Figure 13. Setup to used achieve pulse overlap using third harmonic signal

Generating this third harmonic posed a significant challenge. As mentioned previously, due to the nature of this setup, there were many inherent degrees of freedom in this system. The third harmonic can only be produced in this crystal if all the conditions are correct to a reasonably degree of accuracy. The two most important conditions are the beam co-linearity and pulse overlap in time. To achieve an approximate co-linearity, a limiting aperture was placed in the beam path and the beam was propagated approximately 4 meters so that the red and blue components could diverge significantly were they not collinear. The two beams then needed to be aligned in both the near field and the far field. The adjustment process was iterative and required many hours of adjustment for an optimal result.

Once the beams were approximately collinear, the next step was to vary the delay until a signal was detected at the third harmonic frequency. Since the pulse overlap was previously measured using the streak camera, this phase was somewhat simplified due to the fact that a fixed minimum and maximum delay were already determined for the delay stage. This provided a limited range over which the overlap could occur. However, the BBO crystal is extremely sensitive to the angle of alignment along both the vertical and horizontal axis due to phase-matching conditions. Therefore, a minimum of three parameters required adjustment for approximately every 10 microns of change in the delay. However, once the pulse overlap was detected, optimization of the signal was very straight forward and was accomplished by simply measuring the relative peak intensity of the third harmonic on the spectrometer. Once the third harmonic was optimized, the focusing parabolic was removed for the next phase of the research.

As mentioned previously, achieving an optimized pulse overlap in the BBO crystal was not sufficient for the generation of THz in the plasma. The final adjustment to the system consisted of detecting the third harmonic in the plasma itself. This was accomplished by simply measuring the specular reflection off the filter used to isolate the laser from the THz detector with the Ocean Optics Spectrometer. Figures 14 and 15 show a sample of the spectrum measured during this experiment. As can be seen in Figure 14, the intensity of the third harmonic is significantly lower than either the fundamental or the second harmonic. However, by zooming in, as is done in Figure 15, the third harmonic at 266 nm can easily be identified. It should be noted that the existence of this peak is extremely sensitive to any change in the system parameters.

Even a slight adjustment to the position of the mirrors or the delay stage results in a loss of this peak.

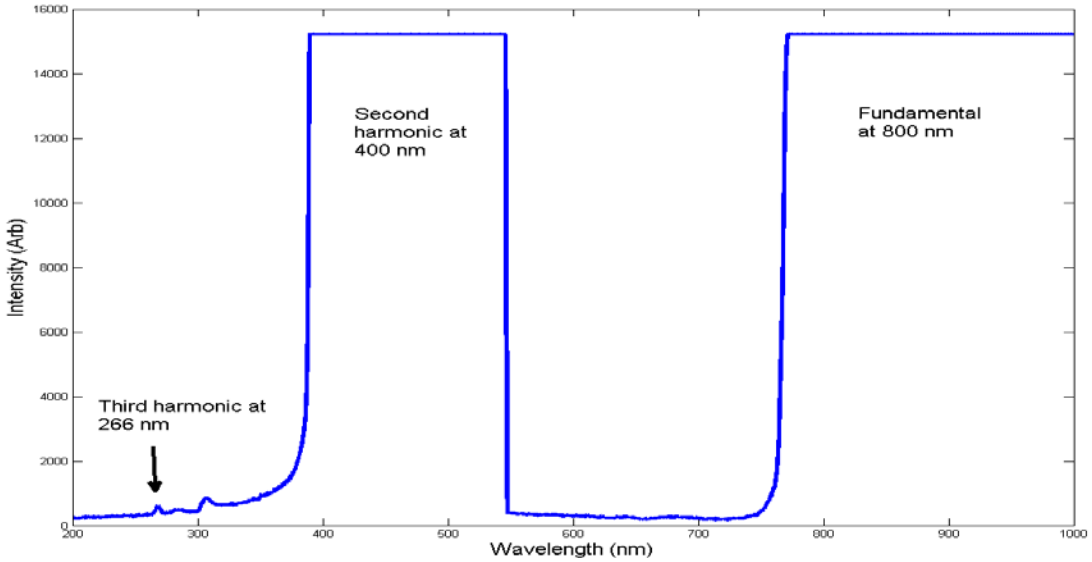

Figure 14. Overview spectra collected on the third harmonic generated by the plasma

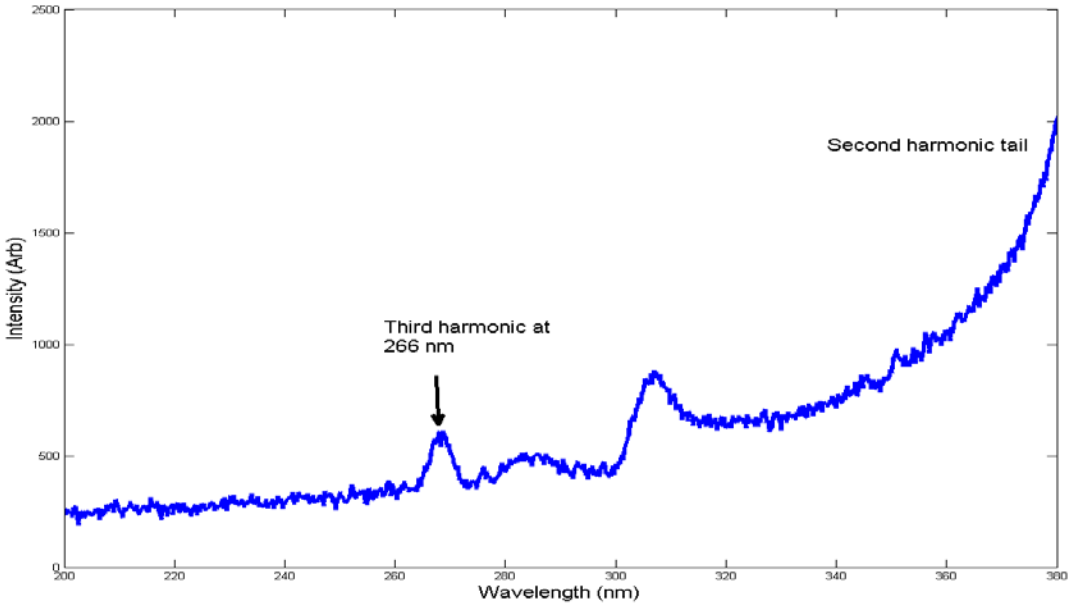

Figure 15. Zoomed in view of the spectra for third harmonic generated by the plasma

4.4 Final Characterization of Plasma and THz

The final phase of this research was by far the most important. All previous experiments were simply necessary steps to be performed in order to make these measurements. The goal of these experiments were as follows:

1. First and foremost; show that it is not only possible, but practical to use a high repetition rate, low peak intensity, ultrashort pulsed laser, utilizing a very short focal length mirror, to generate a THz signal strong enough to be used as a source for THz imaging and spectroscopy.
2. Characterize the relationship between the plasma signal and THz signal in order to determine the feasibility of using the ultrasonic transducer detection method as an inexpensive alternative for indirectly measuring the THz signal.
3. Characterize the effect of the delay on both the plasma and THz signal in an effort to separate the THz production mechanisms and approximate the strength of each of these mechanisms.
4. Measure the change in THz output achieved when an electrical bias is applied across the plasma to determine the feasibility of using modified system with a bias as a strong THz source.
5. Measure the change in both the THz signal and plasma signal as the polarization of the red component is rotated when compared to the blue in an effort to determine the importance of polarization on THz production.

These goals were accomplished through a series of several experiments to be detailed below. However, before a discussion of the various experiments takes place, it should be noted that the experiments performed to achieve the above goals did not necessarily

occur in the order listed. In fact, it was not until near the end of this research that a detectable THz signal, which was dependent on the pulse overlap, was found without the use of the applied bias. The adjustments necessary to achieve this result were cumulative and were only achieved after many hours of "tweaking" the system to increase the signal present with the bias applied. However, once the signal was detected, only minor adjustments were needed to increase the total signal significantly. Therefore, many of the experiments which were performed prior to this achievement were repeated after the system was optimized. It is this data which will be presented.

Many unsuccessful attempts were made to detect THz from an unmodified plasma early in this research. Due to these failures, it was determined that the likelihood of detecting a signal should increase if a bias was applied across the plasma. Previous researchers had demonstrated a 32 fold increase in the average THz output with an applied bias across the plasma [3]. Figure 16 shows a simple schematic illustrating the setup for this experiment. This bias did indeed increase the THz signal to detectable level and allowed for further adjustments to me made to increase the signal. Once the system was adjusted so as to produce a strong THz signal without the bias applied, several experiments were performed to accomplish the objectives listed above.

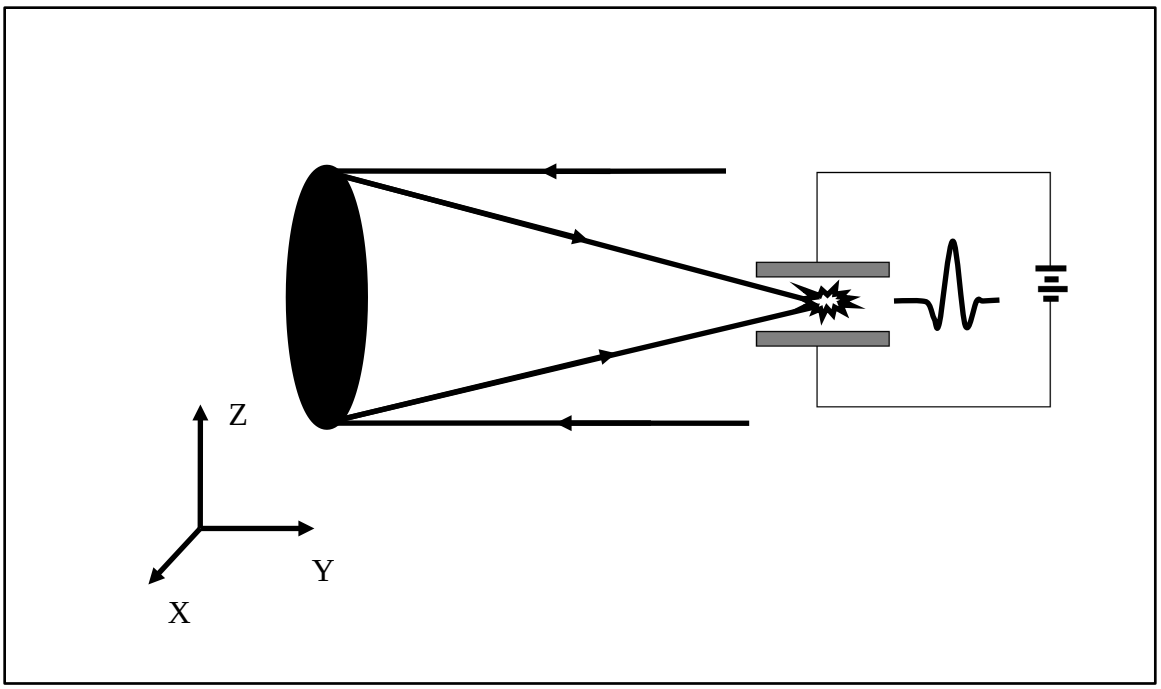

Figure 16. Simplified schematic showing orientation of laser and applied electric field

The first of these experiments was to characterize both the plasma and THz signal as the delay between the red and the blue pulses was varied. This experiment was performed with both the bias applied to a maximum value of 3000 V, equivalent to 27 kV/cm, and with the bias off. The bias voltage was limited to a maximum of 3000 V due to the fact that any higher voltages would result in an electrical discharge between the electrodes because of the dielectric breakdown in air.

The next experiment performed consisted of characterizing the effect of the difference in the polarization of the red and blue pulses to the plasma and THz signals. This was accomplished by rotating the waveplate illustrated in figure 6 through 360 degrees while measuring the change in signal strength of both the plasma and THz simultaneously. The purpose of this experiment was to determine to what degree a

change in polarization affects the THz signal and if the plasma signal reacts in a similar manner.

After characterizing the effect of polarization on the plasma, the effects of the bias on the THz and plasma signals were measured. This experiment consisted of changing the bias from 0-3000 V while simultaneously measuring both the plasma and THz signal. No changes were made to this experiment as compared to the previous except that the waveplate was returned to the position which generated the maximum plasma signal which also corresponded to the maximum THz signal. The data for this experiment was collected over a 10 minute period, where the bias was increased by 100 V every 20 seconds.

Once the relationship between the plasma and the THz signal with respect to the bias voltage was determined, the next step was to determine the effect of each of the two input beams on the THz signal. This experiment was performed with the bias set to 3000 volts to provide the maximum plasma and THz signal. The experiment consisted of blocking the red and blue components of the input beam separately and measuring the change in signal for the plasma and THz signal. The purpose of this experiment was measure how much each of the two components contributed to the overall THz signal and to see if the change in THz signal was evident in the plasma signal. If there was no change when one component or the other was blocked, then it could be assumed the interaction of the two pulses was not the mechanism responsible for the production of the THz. If there was a fractional change in THz output then it could be concluded that more than one mechanism was responsible for the THz production.

The final experiment from this set consisted of measuring the effects of the pulse delay on the THz signal. The purpose of this experiment was almost identical to the previous experiment. The only difference was that this experiment was also performed with a 0 bias voltage to demonstrate that THz production is possible even without a bias voltage using this setup. The basic method for this experiment consisted of simply altering the delay on the delay stage while collecting data on both the THz and plasma strength. As just mentioned, this was done at both 0 and 3000 V bias.

V. Experimental Results and Analysis

5.1 Characterization of Plasma and THz

Figure 17 shows the results of the measurement taken by the streak camera on the plasma lifetime. The primary peak in this plot is the result of bleed through from the laser. However, the tail of the plot represents the plasma lifetime. As you can see on the plot, an exponential fit to this tail gives a plasma lifetime of 279 ps. Other researchers have reported plasma lifetimes of approximately 200 ps [28]. However, the error on these types of measurements is quite high due to the fact that the lifetime changes depending on where you choose to start your exponential fit to the data.

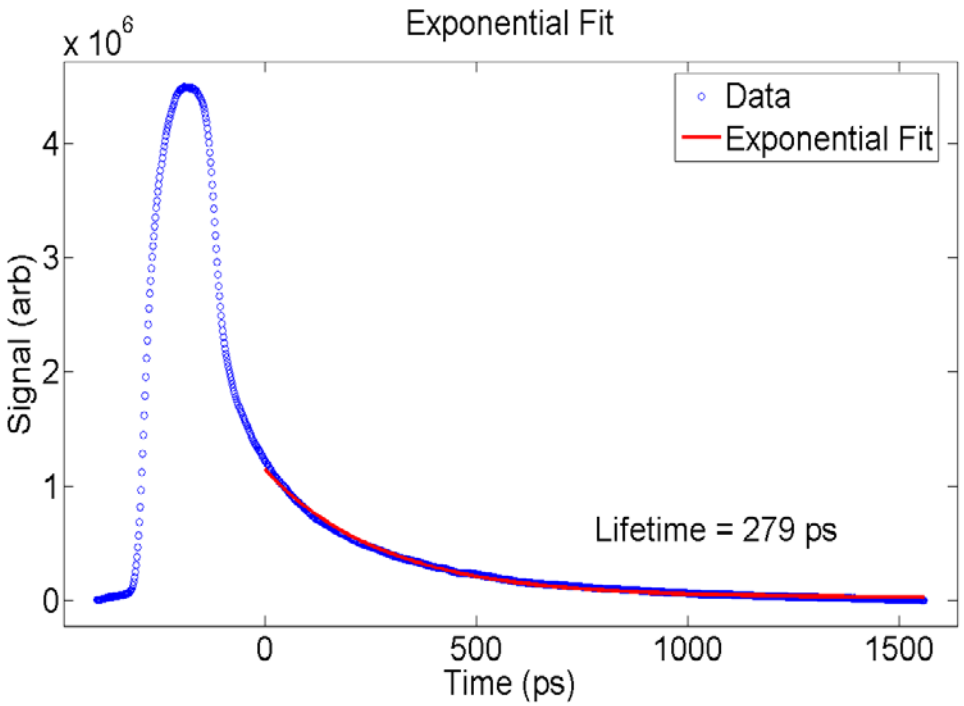

Figure 17. Plasma lifetime

The data collected for the plasma and THz intensity vs the bias voltage can be seen in Figure 18 and Figure 19. The most notable feature in these plots is the clustering of the data. This clustering is simply the result of the collection method. Upon close

examination, especially in the plasma data, you can see the jump from one voltage to the next as the bias was increased. Had it been possible collect the data in a more continuous fashion, this clustering would not have been visible.

Another obvious characteristic of these data is the fact that the two signals appear to be following different curves. To better observe this difference, both datasets were normalized and plotted together as can be seen in Figure 20. The relationship between the plasma vs bias appears to be more nonlinear than THz vs bias. The plasma signal is likely nonlinear due to the fact that the dielectric breakdown of air occurs nonlinearly. However, based on theory, the THz signal should increase linearly as the external bias increases [3]. One possible explanation for this discrepancy is that the air is not fully ionized by the laser at lower bias voltages. As the bias voltage increases the electron density increases and enhances the THz signal. Since the plasma signal increases non-linearly, it would be expected that they THz signal would follow in a similar fashion.

It is interesting to note that even though the THz data is much more linear than the plasma data, it is definitely not linear. This fact is important because previous researchers have claimed that the relationship between THz and bias voltage is in fact linear [3]. However, when you compare their results to those obtained in this experiment, you will notice that the range over which they varied the bias was more than an order of magnitude lower than in this work (0-1.2 kV/cm as opposed to 0-27.1 kV/cm). Therefore, this nonlinearity was not apparent over that much smaller range.

Even though the plasma and THz signals do not change in exactly the same manner, it is clear that both signals increase somewhat in step up to the dielectric breakdown of air. This effect is significant for two reasons. First, the plasma signal can

be used as a reasonable indicator of THz power throughout this range. Therefore, once you have an air plasma THz system functioning with a reasonable THz signal, you can use an inexpensive ultrasonic transducer and lock-in amplifier as a means of measuring the THz output. This saves a significant amount of time and effort needed to set up and operate most THz detection systems. The primary condition for this method to work, however, is that the plasma signal must change with the pulse delay. If this condition is not met, you are not generating THz, and this method is invalid. Secondly if you can somehow alter the breakdown voltage of air it should be possible to increase your plasma signal. One possible technique to achieve this would be to use xenon as opposed to air.

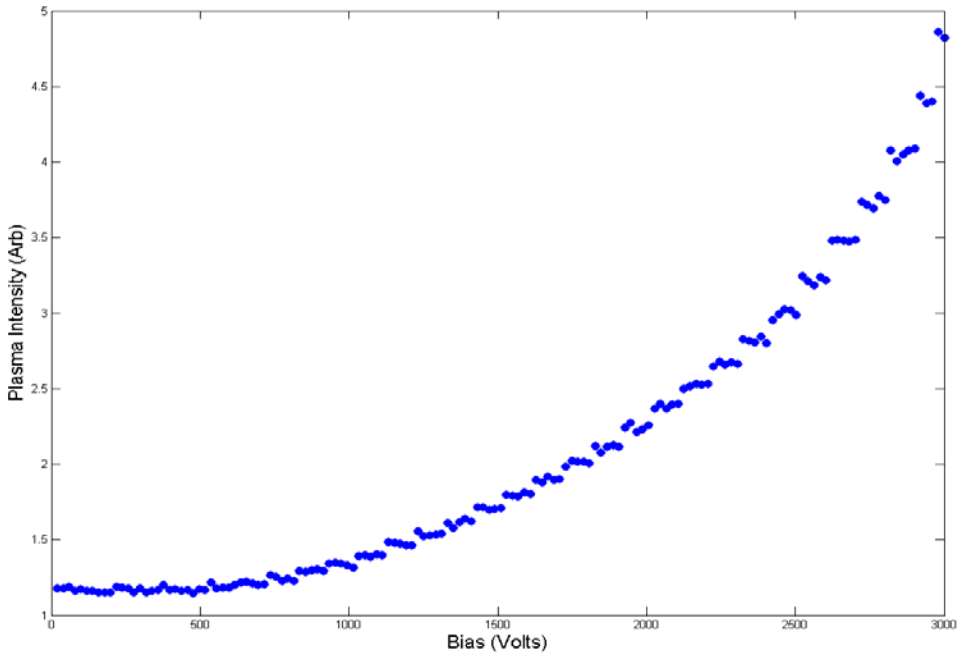

Figure 18. Plasma intensity vs bias voltage

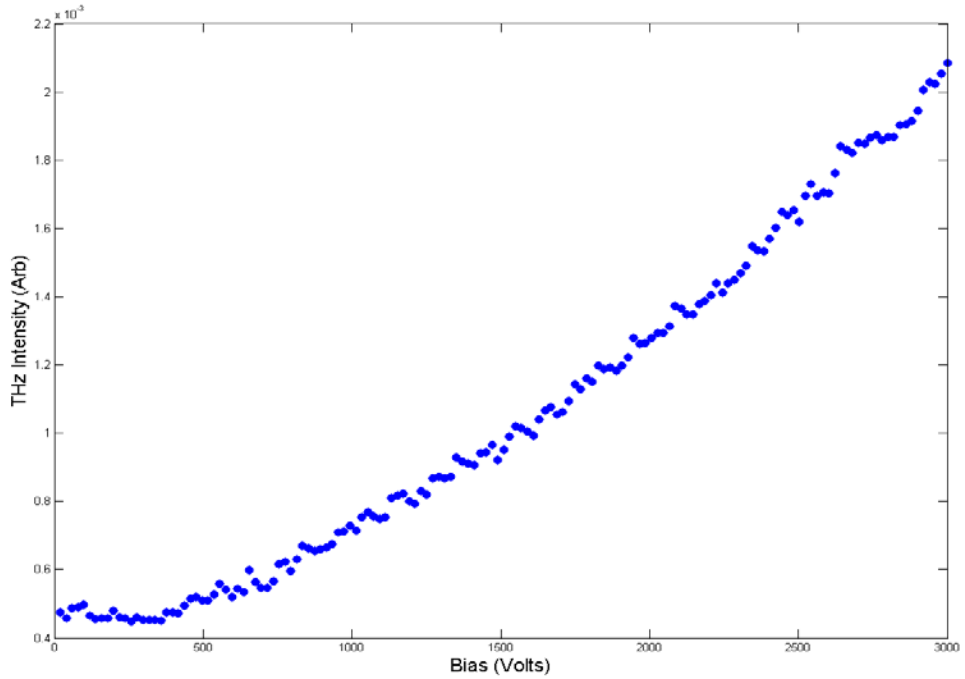

Figure 19. THz intensity vs bias voltage

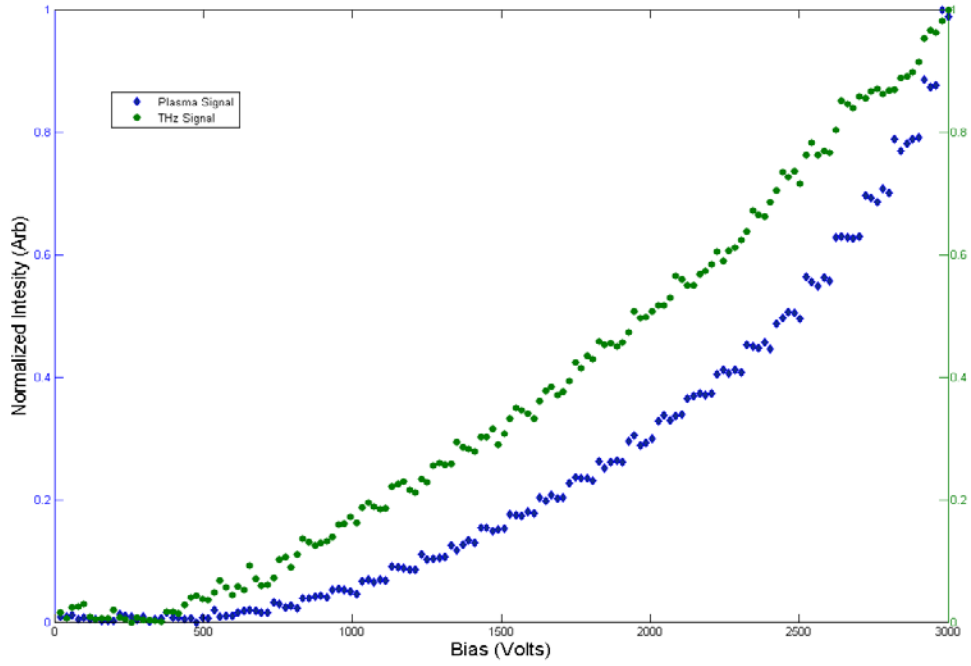

Figure 20. Normalized plot of THz and plasma intensity vs bias voltage

As mentioned previously in the methodology section, two sets of experiments were performed in an effort to determine the number and types of THz production mechanisms occurring in this system. The data from this set of experiments is shown in figures 21-28. Figures 21 and 22 show the data collected on the plasma and THz signals vs a change in the pulse overlap with an applied bias of 3000 V. Figures 23 and 24 show the results of the same experiment except with no bias applied. Unfortunately, a direct comparison between these plots cannot be made since the data for each set was collected at different times under slightly different operating parameters. However, some qualitative comparisons can be made. For instance, it is apparent that the plasma intensity is higher at the leading edge of the pulse overlap than the trailing edge, whereas the THz signal appears to be the same on both sides. Unfortunately the physical mechanism responsible for this effect is not known and was not further studied since it had no apparent effect on the THz signal but it may have interesting implication to other fields of research.

Upon careful examination of figures 22 and 24, it can be seen that a background THz signal exists even without pulse overlap. This effect is most noticeable when the bias is applied. The fact that this signal exists without the overlap suggest that a one of the previously discussed production mechanisms is responsible, the ponderomotive force, or the resonant plasma oscillation due to radiative pressure. It is very likely that each method contributes a fixed amount to this signal and that this contribution changes with both the bias and the degree of pulse overlap. However it is not possible to verify this statement with the data collected. If future studies are conducted, it is likely that these mechanisms can be isolated and quantified by measuring the polarization of the output

THz pulse. It is very likely that each of these production mechanisms generates THz with differing polarizations.

A peak to floor ratio can be calculated for the THz from these plots. The peak to floor ratio for THz production without an applied bias was 5.6 whereas when a bias was applied this value drops to 2.9. The difference is due to the fact that a significant THz background signal was present when the bias as applied. However, by achieving a perfect pulse overlap, this background THz signal was increased by a factor of 3. This increase suggests that even though THz production is possible without perfectly overlapping the pulses, to achieve the maximum usable signal, this overlap is a requirement.

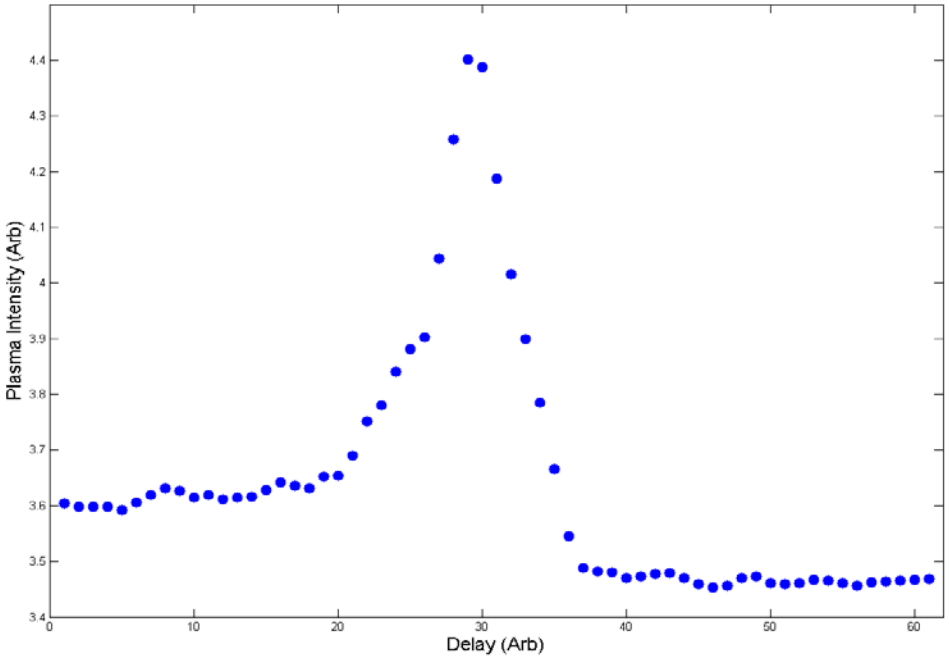

Figure 21. Plasma intensity vs pulse delay with 3000 V applied bias

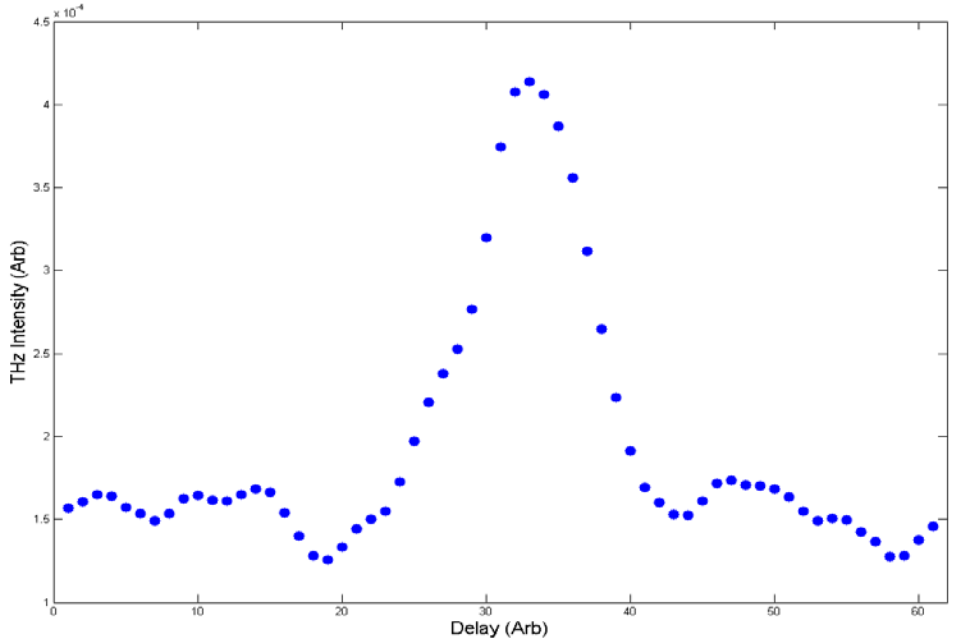

Figure 22. THz intensity vs pulse delay with 3000 V applied bias

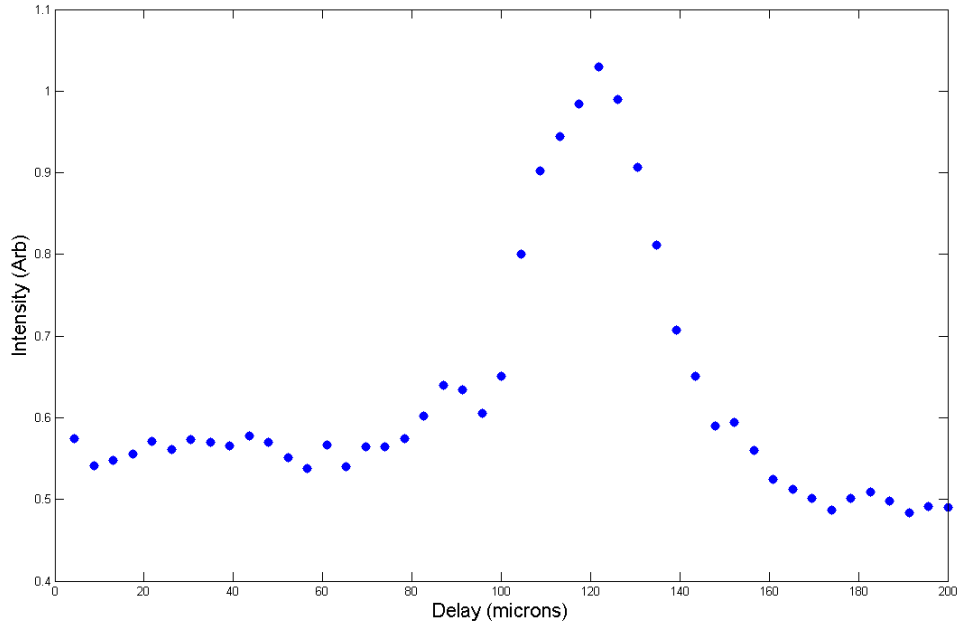

Figure 23. Plasma intensity vs pulse delay with no applied bias

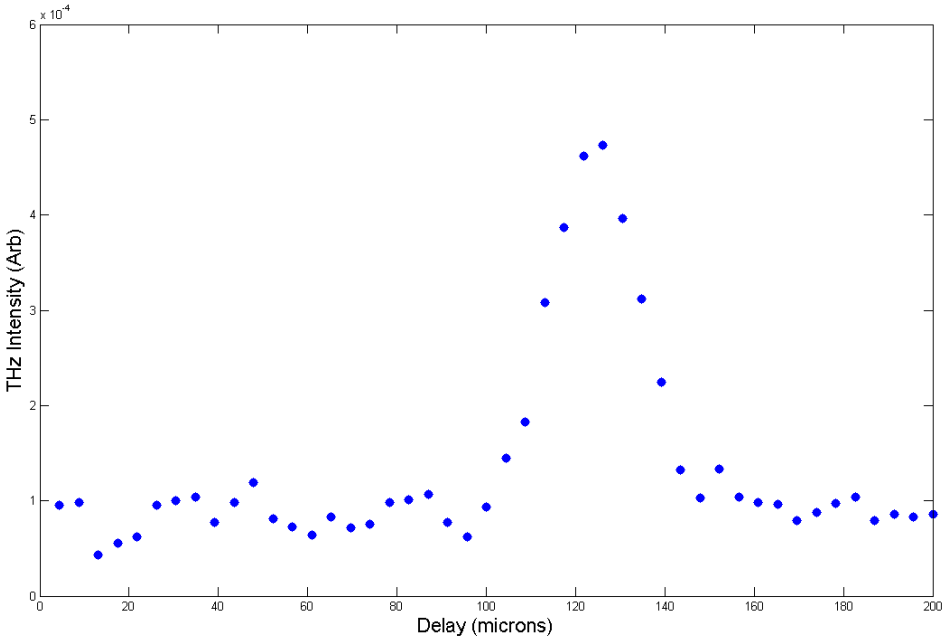

Figure 24. THz intensity vs pulse delay with no applied bias

The change in both the plasma and THz signals when either the red or blue components of the beam are blocked is illustrated in Figures 25 and 26. These measurements were taken with an applied bias of 3000 V. It is apparent from Figure 25 that the plasma signal was generated mostly by the blue component of the laser and cannot be sustained by the fundamental alone. Therefore, the change in THz signal when the blue component is blocked will obviously go to zero as well since the existence of the plasma is a requirement for THz production. However, when the red component is blocked, it can be seen that there is only a slight decrease in the plasma signal but a much more significant change in the THz signal. This change agrees well with the change observed when the delay between the two pulses was altered in the previous experiment. There is again, approximately a 300% increase in the THz signal when both components

are present as opposed to the presence of only the blue component. Also, as before, it can be seen that the signal does not go to zero when the red is blocked. Again, this is likely due to the fact that a secondary production method is responsible for the production of THz.

This data was also used to calculate an approximate signal to noise ratio for the THz signal. This was accomplished by taking the standard deviation of the data with both components present and dividing it by the mean of the same subset of data. The result of this calculation gave a signal to noise ratio of 13.

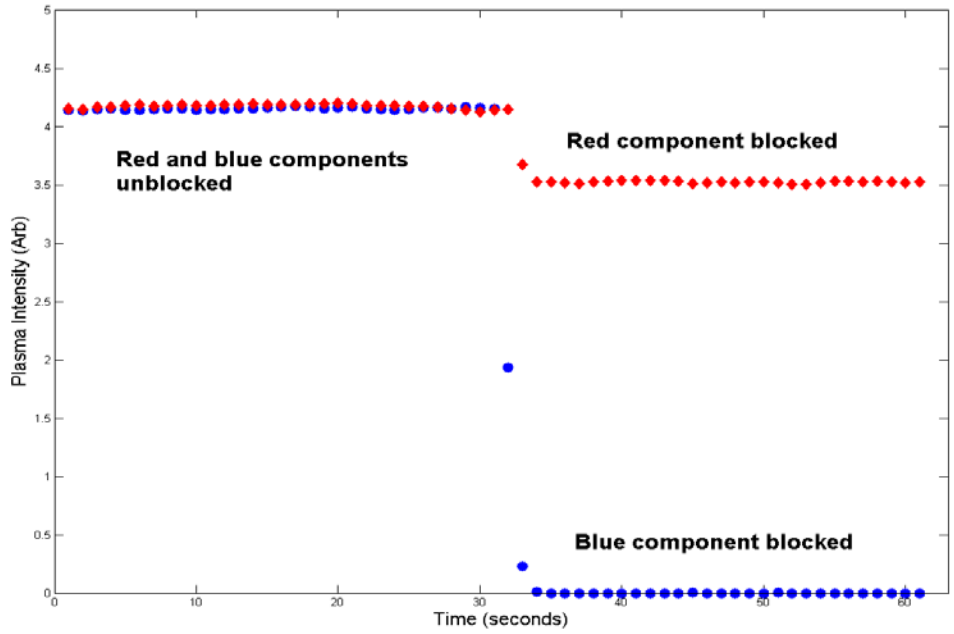

Figure 25. Change in plasma intensity when each component is blocked independently

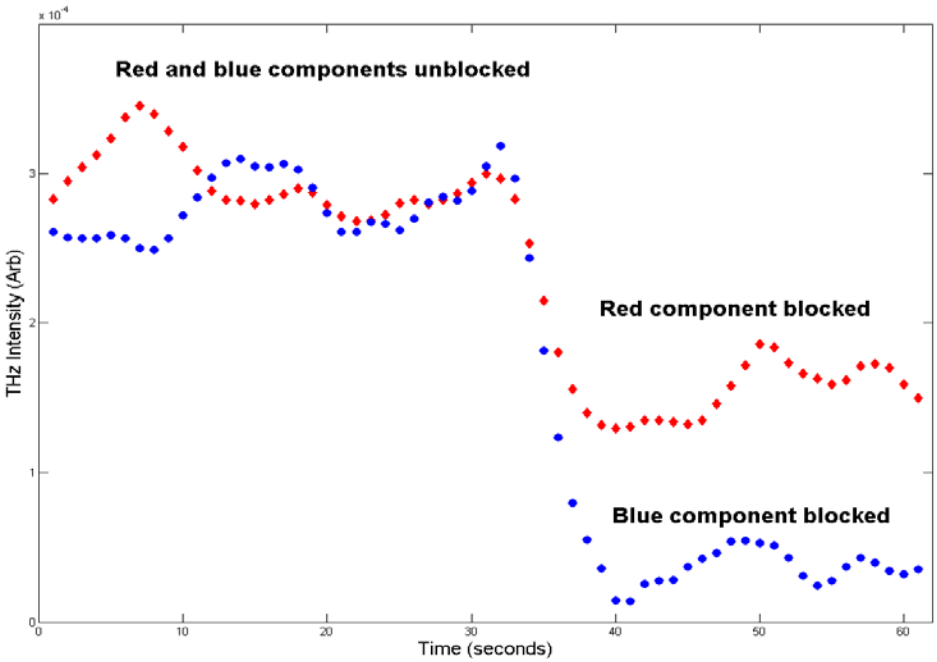

Figure 26. Change in THz intensity when each component is blocked independently

The change in both the THz and plasma signals as the polarization of the red component of the beam is rotated is illustrated in Figures 27 and 28. The data was collected as the polarization was rotated from a point where the plasma signal was maximized through 360 degrees. This experiment was conducted with the bias voltage set to 3000 V for the maximum signal quality. It can be seen immediately when comparing the two plots that the THz signal was much noisier than the plasma signal. It is also obvious that the THz data falls off significantly as throughout the collection while the plasma data remains fairly consistent throughout. This is likely due to either a fluctuation in the laser parameters during the course of the collection or a change in the laboratory environment such as an increase in humidity. Any slight variation in the laser output tended to have a larger impact on the THz signal than the plasma signal.

The angle between each successive peak and trough can be calculated by taking the total number of peaks and troughs and dividing the result by 360 degrees. This method is necessary due to the fact that this collection was made by manually rotating the waveplate by hand. Therefore, the data varies throughout the collection but on average is accurate. The result of this calculation shows that the average angle between peaks and troughs is 45 degrees. This result is consistent with the rotation of a half wave plate through 360 degrees since a half waveplate will give a maximum intensity when the polarization of either the fast axis or slow axis is aligned with the polarization of the field. This gives a total of four maximums and four minimums for every 360 degrees of rotation which is in good agreement with the calculations.

Due to the noisy nature of the THz data, it is difficult to determine if it corresponds to the plasma data. However, upon close examination, there appear to be peaks and valleys which directly correspond to the plasma data. This data again verifies that the plasma signal is a reasonable indicator of the THz signal so long as the previously mentioned conditions are met. It also demonstrates that the polarization between the red and blue components is critical to maximum THz production. However, it is not apparent whether this is the result of better mixing between the red and blue components or simply the direct result of a stronger plasma signal. An interesting follow on experiment would be to repeat this experiment while using a second laser to generate the plasma so that you could decouple the increase in plasma signal from the change in THz signal.

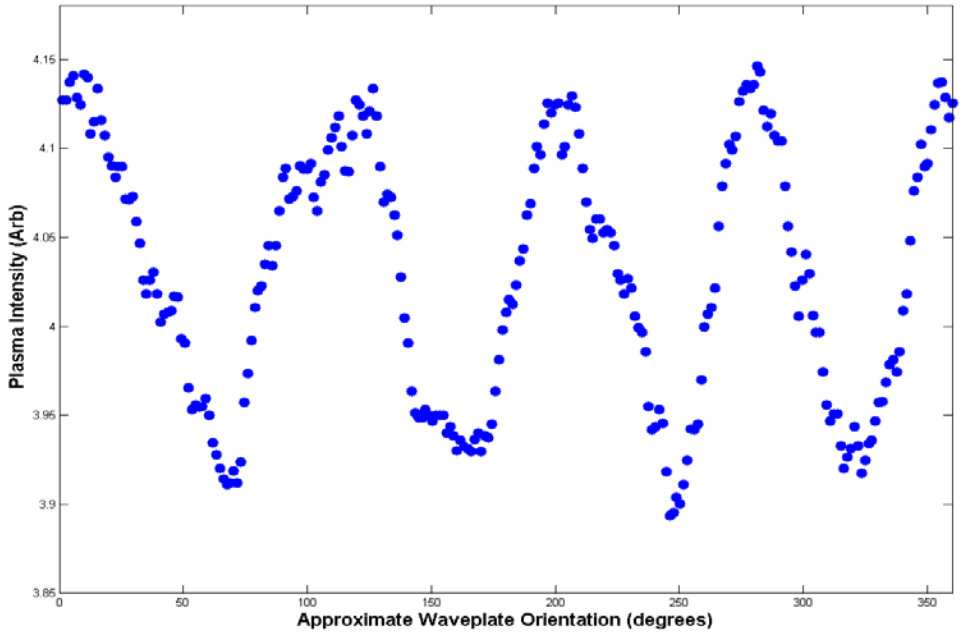

Figure 27. Plasma intensity vs polarization with 3000 V applied bias

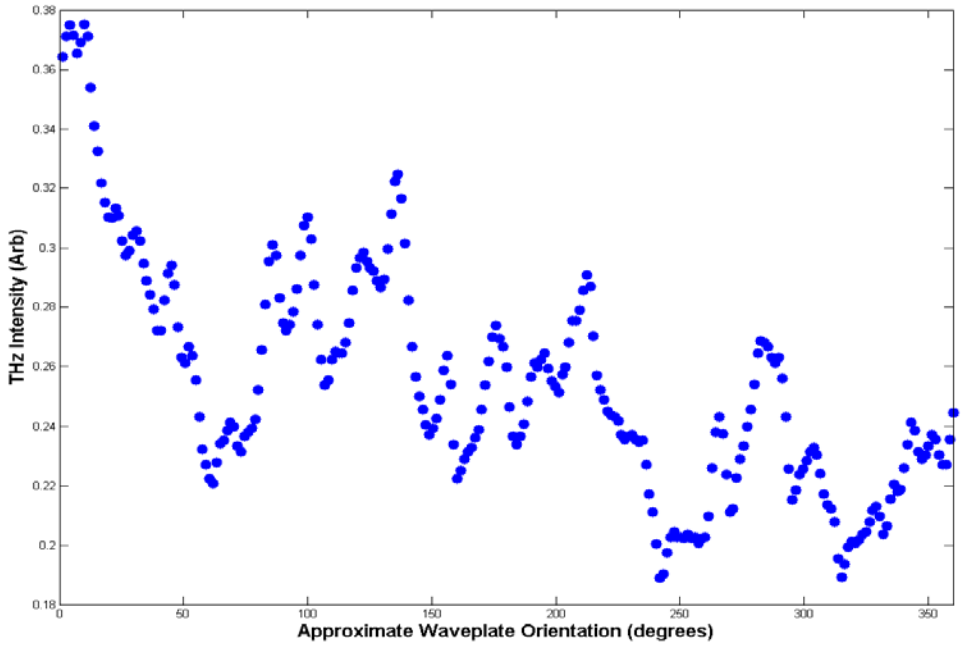

Figure 28. THz intensity vs polarization with 3000 V applied bias

5.2 Effects of Silicon Filters and the Implications

During the course of this research, the primary means of isolating the laser from the THz dector was through the use of a Microtech® Instruments Inc. THz Low Pass Filter. The spectral characteristics for this filter are illustrated in Figures 29 and 30 for both the THz region and the visible to IR region. As you can see from the plots, the filter passes THz over a fairly broad spectrum while almost completely blocking the IR. However, there is some transmission of the blue light at 400 though this transmission in the blue had very little noticible impact on any of the experiement performed.

The reason for discussing this filter is because several groups in the community doing very similar research tend to use silicon filters instead of this type of filter due to the fact that they also block the red component of the beam quite well and are fairly inexpensive compared to the filter used in this work. However, it was discovered during the course of this research that silicon can be a significant source of THz as well.

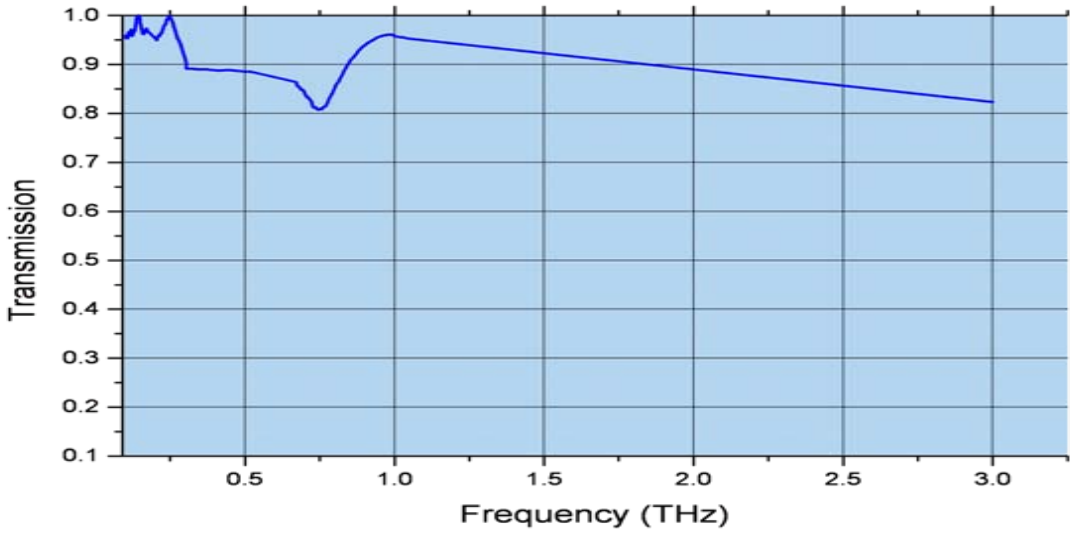

Figure 29. THz low pass filter THz transmission spectrum

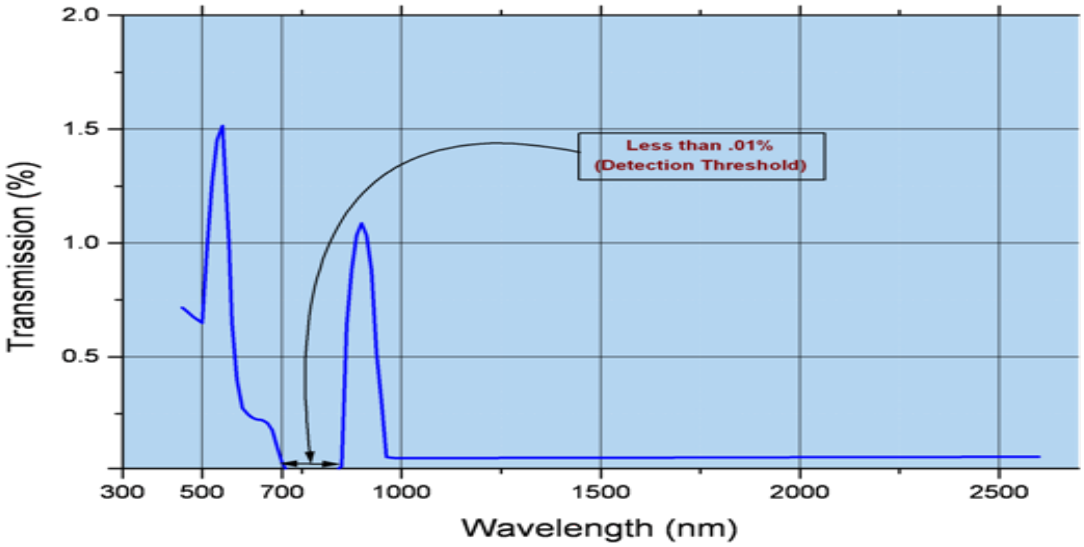

Figure 30. THz low pass filter visible to mid IR transmission spectrum

The THz production capabilities of a silcon filter was characterized by an additional, unplanned experiment and is illustrated in Figure 31. During this experiment, the THz signal was optimized with an appied bias of 3000 V. The silicon filter was then placed in the beam path between the two parabolic mirrors. The beam, which was collimated to approximately the original beam width, impinged on the surface of the silicon. A second filter (the one described above) was placed between the second parabolic and the detector to prevent saturation of the detector. This filter was in place for the entire experiment.

The data shows the change in the THz signal with the filter in place and the filter removed. As can be clearly seen, the THz signal is nearly an order of magnitude higher when the filter is in place than when it is not. In fact, this signal was larger than anything produced during the course of this research. It was determined that the THz produced by the filter was generated by the blue component of the beam only. This fact might explain why this phenomena has yet to be reported. Many of the air plasma THz experiments

that have been peformed previously only used the fundamental frequency. It is only more recently that research involving the second harmonic as well the fundamental has become popular. Therefore, it is likely that many researchers who evolved from working with only the fundamental to both the fundamental and second harmonic, assumed that the filter would work equally well and did not attempt to determine if the filter itself might contribute to the THz signal.

It is not perfectly clear at this time what mechanism is responsible for the production of THz in silicon. However, previous work has suggested that it might be the result of the photo dember effect [29].

As a result of these measurements, it is highly recommended that silcon filters not be used in research whose goal is to produce THz by some other means. It is also recommended that the nature of THz production be studied in more detail so as to characterize the nature of this radiation to determine its feasibility as a source. Due to time constraints and the fact that this discovery came at near the end of this research, these experiments were not possible as part of this work.

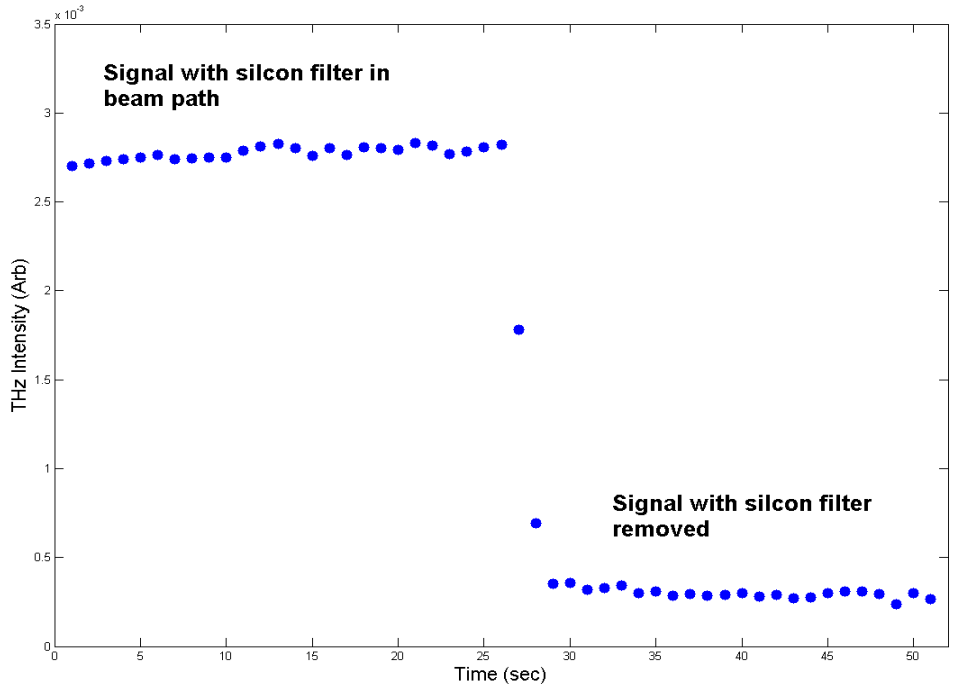

Figure 31. Change in THz signal when a silicon filter is placed in the path of the beam

VI. Future Work

Quite a lot of data was collected during the course of this research. However, there is still a significant amount of work that should be accomplished. The first step would be to characterize the both the spectrum and polarization of the THz produced by this system. Acquiring good data on these two properties would provide a better understanding of the mechanisms responsible for THz production. In addition, an entire suite of experiments could be performed in an effort to increase the THz signal by varying the repetition rate of the laser, varying the temperature, pressure, or composition of the medium in which the plasma is being generated, as well as varying the angles in which the red and blue components of the beam mix. In addition, a full characterization of the silicon filters should be performed to determine the nature of the THz produced and the possible applications as a means of production.

VII. CONCLUSION

The primary objective of this research was to generate a detectable THz signal using ultrashort pulsed laser with a high repetition rate and low peak pulse energy as a potential source for high speed THz imaging and spectroscopy. This objective was definitively achieved, initially by using an applied external electric bias across the plasma, and subsequently with no applied bias. Once a measurable signal was generated, several experiments were performed in order to characterize the THz signal as well as the relationship between the THz and plasma signals.

The first of these experiments measured the plasma lifetime using a high speed streak camera. An exponential fit of the data acquired gave a lifetime of 279 ps, a value consistent with previously measured results using alternate methods.

The relationship between both the THz and plasma signals was also measured. The results show that both signals increased nonlinearly as the applied bias was increased. These results, specifically regarding the nonlinearity of the THz, were initially inconsistent with previously reported results. It was determined that these results are likely caused by an incomplete ionization of the air caused by the relatively low peak pulse powers generated by this system. A second series of experiments characterized the significance of the pulse overlap to the generation of THz as well and demonstrated that multiple effects were responsible for the generation of THz, specifically when an external bias was applied. It was also demonstrated that both the THz and plasma signals were significantly affected, and changed in step, when the polarization between the fundamental and second harmonic was varied.

Finally, as an unexpected discovery, it was found that silicon filters, often used to isolate the THz detector from the laser, were a significant source of THz radiation when exposed to the second harmonic beam. The implications of this discovery are significant due to the fact that many experiments similar to the ones performed in this research effort have used these filters. This suggests that perhaps some of the data collected during this previous work could have been contaminated by the THz being generated in the silicon filter.

This work represents a critical first step in the production of a high power high repetition rate THz source in a potentially compact package. The development of such a source would enable many applications relevant to the DoD. The most obvious application for this technology is security scanning for both conventional weapons and WMD at critical locations such as airports, ports of entry, and military checkpoints. THz imaging provides not only the capability to visually identify these potential threats, even when hidden, but also provides the capability to quantify these images in such a way that the materials can be identified by their chemical composition. Another important application is the non-destructive testing of composite materials such as those used on many modern military aircraft. Work at AFIT has already demonstrated that THz could be used to identify burns, bends, and delaminations in these composite materials. However, as previously mentioned, these scans take many hours to accomplish due to the low average power resulting from the solid state THz source being used. Other suggested applications for this technology include secure short range communications in the earth's atmosphere possible due to the rapid attenuation of THz in the atmosphere as well as

secure satellite to satellite communications, covert terrain mapping for aircraft in brownout situations, and remote detection of nuclear effluents for treaty monitoring.

APPENDIX A. OPERATING INSTRUCTIONS FOR THE SILICON BOLOMETER

This appendix is meant to be used as an supplement to the manufacturers operating instructions based on my experiences with the quirks inherent in this specific system.

1. Precooling the detector

a. In my experience, it is best to place the detector at about 3 feet above the floor when filling it with liquid nitrogen. However, using the current setup, the detector must be filled in place while hooked up to a vacuum pump. I recommend a sturdy stool for the filling process since the storage dewar can become quite heavy during the filling process.

b. Put on all appropriate PPE and continue wearing it for the remainder of this process.

c. Ensure all valves between the detector and the mechanical pump are open and the detector valve itself is closed.

d. Turn the mechanical vacuum pump on and wait for the green light to come on indicating the pump is up to speed. This takes about 5 minutes.

e. Turn the turbo pump on. Wait for it to come up to speed.

f. Slowly open the detector valve.

g. Insert tube (A) into the center port and (B) into the outer port.

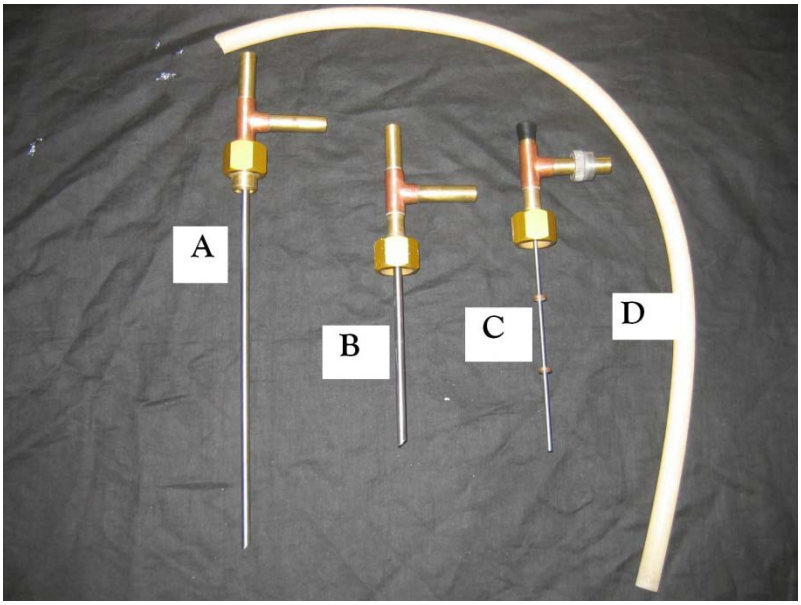

h. Next place the funnel in tube (A) and slowly fill the bolometer with liquid nitrogen. Once full, liquid nitrogen will begin to spill out the side port in the tube. During the filling process the dewar sometimes undergoes a rapid change in temperature which results in liquid nitrogen spewing out of the tube violently. This effect is usually preceded by an significant increase in the off gassing from the side port. Be aware of this effect and be careful when it happens since liquid nitrogen will often spray a few feet in the air. Once this occurs, top off the dewar and move to the next step. It this does not happen, simply move to the next step and watch for it carefully because sometimes it does not happen until you begin filling the outer dewar.

i. Once the inner dewar is filled place the funnel in tube (B) and repeat the process for the outer dewar. The outer dewar will also spray liquid nitrogen just like the inner dewar so be cautious. If the inner dewar did not vent violently while it was being filled it will happen at this step. When it happens, simply top off the inner dewar and continue filling the outer dewar until it vents. Once it vents, top it off and then wait approximately an hour before moving to the next step.

    i. Note: If, by chance, you have water accumulated in either of the dewars, they will not fill with liquid nitrogen. The liquid nitrogen will simply boil off as fast as you can fill it. If this happens, blow out the dewar using dry nitrogen or helium by placing a hose on the vent port. Continue this until no sign of water comes from the fill portion of the tube.

2. Filling the detector with liquid helium

a. Once the detector has adequately precooled (approximately 1 hour after filling with liquid nitrogen) you can fill it with liquid helium. Before you can fill it with liquid helium the liquid nitrogen must be removed from the inner dewar. To accomplish this, place the rubber hose labeled (D) over the top of tube (A) which is inserted in the inner dewar.

b. Next, place the end of this hose into the storage dewar you used to fill the detector with liquid nitrogen. You do not have to do this, but it allows you to recover most of the liquid nitrogen you used to pre-cool the detector. You can also simply blow the liquid nitrogen out onto the floor where it will evaporate but the practice is wasteful and I don't recommend it.

c. Once the tube is in the dewar, blow out the vent port with either dry nitrogen or helium gas. The liquid nitrogen will flow into the container. This step takes about 1 minute and you know the detector is empty when the liquid nitrogen stops flowing from the tube.

i. Note: The next step in the process should be completed rather quickly to prevent unnecessary warming of the now empty inner dewar.

d. First remove the tube (A) from the detector leaving the rubber hose connected since it is frozen stiff at this point.

e. Move the helium dewar into place a few feet from the detector and insert the helium transfer tube into the dewar.

f. Close the valve leading to the low pressure release valve on the helium dewar.

g. Lower the helium transfer tube into the helium dewar very slowly (approximately ½ inch every second) while ensuring the other end of the hose is facing away from you.

i. Note: You can lower it significantly faster for about the first 3 or 4 feet. However, once you reach liquid helium, you must lower it slowly or else you will rapidly heat the liquid helium in the dewar which will result in a significant pressure increase in the dewar which will then be relieved quite loudly by the high pressure release valve on the dewar. This is scary and I don't recommend it.

h. When the hose reaches liquid helium, there will be a change in the sound of the gas exiting the tube. The hissing sound will begin to oscillate. At this point you can place the end of the hose into the inner port on the detector. The hose will go all the way to the bottom of the detector.

i. Continue lowering the transfer tube into the dewar very slowly. Monitor the pressure at the valve on the helium dewar. You do not want this pressure to exceed 5 p.s.i. If it does, you will not be able to fill the detector and will have to remove the tube from the detector, relieve the pressure, and start again. The pressure will remain steady so long as you continue to lower the tube at approximately ½ inch per second. Continue lowering the tube until it reaches the bottom of the dewar.

j. Once the transfer tube reaches the bottom of the dewar, Liquid helium should be flowing and cooling the detector. The liquid helium will simply evaporate on contact until the detector reaches the appropriate temperature. During this phase there will be significant off gassing. However, if you have done everything correctly to this point, the off gassing will be steadily decreasing in intensity and will eventually stop completely for a few seconds. This transition is very noticeable and happens after about 5 minutes from the time liquid helium is flowing.

k. Once the liquid helium begins to collect in the detector, you will notice continued off gassing but it will be significantly reduced when compared to

the cooling phase. After about 3 minutes, the dewar will fill and you will notice another change in the gas exiting the detector. It will have the appearance of a boiling cloud. The gas will be very billowy and thick.

l. When you are satisfied that the detector is full of liquid helium, quickly remove the transfer tube from the detector first and then quickly raise the transfer tube from the liquid helium portion of the helium dewar.

   i. Note: It is imperative that you remove the hose from the detector first, otherwise when the transfer tube is pulled out of the helium dewar it will begin to flow helium gas which will then blow all the liquid helium out of your detector.

   ii. Once the transfer tube is out of the detector, it is only necessary to remove the tube from the liquid helium portion of the helium dewar rapidly. The reason for this is to prevent excessive loss of liquid helium. Once the hose is in the portion of the dewar filled with gas, you can then remove it from the dewar with more care to prevent to much off gassing and loss of liquid helium.

m. While removing the transfer tube from the helium dewar, ensure that you do so slowly so that you can close the valve prior to fully removing the tube. This prevents rapid venting of the dewar.

n. When the transfer tube is fully removed, stow it back on the cabinet and open the low pressure release valve partially to slowly relieve the pressure in the dewar.

o. Place tube (C) into the inner port on the detector with rubber plug in place.

p. Turn the “Power on” switch to the “On” position on the preamplifier

q. Wait approximately 45 minutes for the detector to reach equilibrium.

3. Pumping on the Helium

a. After allowing the detector time to reach equilibrium, attach the pump tube to the horizontal port on the tube.

b. Tighten the swage lock connector hand tight

c. Tighten the tube to the detector with at wrench. Do not over tighten. During this step it is often helpful to hold both the detector and the tubing in place while tightening to prevent all the various parts from twisting at odd angles.

d. Ensure both valves are closed between the pump and the detector by turning them clockwise.

i. Note: Do over tighten the needle valve, doing so will destroy it so that it will never completely close.

e. Turn the pump on. Wait for it to come up to speed.

f. Hook a cable between the bias voltage connector on the pre-amp and an ohm meter.

i. The ohm meter should be reading approximately 20.3 Mega ohms at this point

g. Open the needle valve fully and wait 30 minutes while the system pumps on the helium bath.

h. After approximately 30 minutes, the pressure on the gauge should be reading between 10 and 15 in Hg. At this point, slowly begin to open the larger valve until you notice in increase in the rate of resistance change. Wait another 30 minutes.

i. The ohm meter should be reading about 20.5 Mohms at this point and should be increasing at about 0.001 Mohm's per every 2-3 seconds.

i. After 30 minutes, continue opening the valve trying to maintain a change of resistance of approximately 0.001 Mohm's per every 1-3 seconds until the pressure gauge reads greater than 25 in Hg or the Ohm meter reads greater than 21.000 MOhm's. At this point you will be at temperature and the detector is ready to operate.

4. Operating the detector

a. Remove the cable from the bias connector

b. Connect a cable between the "Output" port on the pre-amp and the lock in amplifier.

c. Turn "Input on" and "Bias on" switches to the on position (Up)

d. Turn on the chopper and sync the lock in amplifier to the chopper frequency (optimal for this detector is between 10 and 20 Hz) and begin collecting data.

BIBLIOGRAPHY

1. www.picometrix.com

2. Stoik, C., Bohn, M., and Blackshire, J., "Nondestructive evaluation of aircraft composites using transmissive terahertz time domain spectroscopy," Opt. Exp. 16, No. 21, 17051 (2008)

3. Sun, W. F., Zhou, Y. S., Wang, X. K., and Zhang, Y., "External electric field control of THz pulse generation in ambient air," Opt. Exp. 15, No. 8, 15483 (2008)

4. URL: http://www.zomega-terahertz.com

5. Hamster, H., Sullivan, A., Gordon, S., White, W., and Falcone, R., "Subpicosecond, electromagnetic pulses from intense laser-plasma interaction," Phys. Rev. Lett. 71, 2725 (1993).

6. D'Amico, C., Olivier, T., Méchain, G., Franco, M., Prade, B., Pellet, M., Gheudin, M., Mysyrowicz, A., "THz Emission From Electrically Charged Femtosecond Filaments in Air," Opt. Soc. of America, 190.5530, Pulse propagation and solitons, 350.5400 Plasmas.

7. Cook, D. J. and Hochstrasser, R. M., "Intense terahertz pulses by four-wave rectification in air," Optics Letters, Vol. 25, No. 16 (2000)

8. Zhong, H., Karpowicz, N., and Zhang, X.-C.,"Terahertz emission profile from laser-induced air plasma," App. Phys. Lett. Vol. 88, 261103 (2006)

9. Kim, K. Y., Glownia, J. H., Taylor, A. J., and Rodriguez, G., "Terahertz emission from ultrafast ionizing air in symmetry-broken laser fields," Opt. Exp. 15 No.8, 4577-4584 (2007)

10. Hu, B., and Nuss, M., "Imaging with terahertz waves," Optics Letters, Vol. 20, No. 16 (1995)

11. Wu, Q., Hewitt, T., and Zhang, X., "Two-dimensional electro-optic imaging of THz beams," App. Phys. Lett. Vol. 88, 002982 (1996)

12. Mittleman, D., Hunsche, S., Boivin, L., and Nuss, M., "T-ray tomography," Optics Letters, Vol. 22, No.12 (1997)

13. Jiang, Z., and Zhang, X., "Single-shot spatiotemporal terahertz field imaging," Optics Letters, Vol. 23, No. 14, (1998)

14. Diels, J.-C. and Rudolph, W., *Ultrashort Laser Pulse Phenomena*, Academic Press, 2006

15. Yariv, A., and Yeh, P., *Optical Waves in Crystals*, Wiley-Interscience, 2003

16. Kress, M., Loffler, T., Eden, S., Thomson, M., and Roskos, H. G., "Terahertz-pulse generation by photoionization of air with laser pulses composed of both fundamental and second-harmonic waves," Opt. Lett. Vol 29, 1120-1122 (2004)

17. Rodriguez, G., Siders, C., Guo, C., and Taylor, A., "Coherent ultrafast MI-FROG spectroscopy of optical field ionization in molecular H2, N2, and O2," IEEE J. Select. Topics Quantum Electron., vol. 7, 579-591, (2001)

18. Gibbon, Paul., *Short Pulse Laser Interactions with Matter an Introduction*, Imperial College Press, 2005

19. Cheng C C, Wright E M and Moloney J V., "Generation of electromagnetic pulses from plasma channels induced by femtosecond light strings" Phys. Rev. Lett. Vol. 87 213001 (2001)

20. Sprangle, P., Penana, J., Hafizi, B., and Kapetanakos, C., "Ultrashort laser pulses and electromagnetic pulse generation in air and on dielectric surfaces," Phys. Rev. E. Vol 69, 066415 (2004)

21. Houard, A., *et all*, "Strong enhancement of terahertz radiation from laser filaments in air by a static electric field," Phys. Rev. Lett. Vol. 100, 255006 (2008)

22. Kim, K. Y., Taylor, A. J., Glownia, J. H., and Rodriguez, G., "Coherent control of terahertz supercontinuum generation in ultrafast laser-gas interactions," Opt. Exp. 15 No.8, 4577-4584 (2007)

23. Grenouille Model 8-50 User's Guide, Swamp Optics, Atlanta, GA 30339

24. URL: http://www.swampoptics.com

25. IR Labs Silicon Bolometer User's Guide, IR Labs, Tucson, AZ, 85719

26. QMC Instruments Cryogenic Composite Bolometer System Operating Manual, QMC Instruments LTD, The Parade Cardiff, UK

27. Hamamatsu Streak Camera User's Guide, Hamamatsu, Hamamatsu City, Japan

28. Kampfrath, T., et all, "Long- and short-lived electrons with anomalously high collision rates in laser-ionized gases," Phys. Rev. E Vol. 76, 066401 (2007)

29. Xiaodong, M., Ding, Y., "Silicon thin film on SiO_2: an efficient broadband terahertz generator," Lasers and Electro-Optic Soc. The 20th Annual Meeting of the IEEE, Issue 21-25 (2007

REPORT DOCUMENTATION PAGE

Form Approved
OMB No. 074-0188

1. REPORT DATE *(DD-MM-YYYY)*	2. REPORT TYPE	3. DATES COVERED *(From – To)*
26-03-2009	Master's Thesis	Aug 2007 - Mar 2009

TITLE AND SUBTITLE
Production and characterization of high repetition rate terahertz radiation in femtosecond-laser-induced air plasma

5a. CONTRACT NUMBER
5b. GRANT NUMBER
5c. PROGRAM ELEMENT NUMBER

AUTHOR(S)

Dexter, Michael L., Captain, USAF

5d. PROJECT NUMBER
5e. TASK NUMBER
5f. WORK UNIT NUMBER

7. PERFORMING ORGANIZATION NAMES(S) AND ADDRESS(S)
Air Force Institute of Technology
Graduate School of Engineering and Management (AFIT/EN)
2950 Hobson Way, Building 640
WPAFB OH 45433-8865

8. PERFORMING ORGANIZATION REPORT NUMBER
AFIT/GAP/ENP/09-M04

9. SPONSORING/MONITORING AGENCY NAME(S) AND ADDRESS(ES)
Intentionally left blank.

10. SPONSOR/MONITOR'S ACRONYM(S)
11. SPONSOR/MONITOR'S REPORT NUMBER(S)

12. DISTRIBUTION/AVAILABILITY STATEMENT
APPROVED FOR PUBLIC RELEASE; DISTRIBUTION UNLIMITED.

13. SUPPLEMENTARY NOTES

14. ABSTRACT

The purpose of this research was to produce and characterize high repetition rate terahertz radiation in ionized air plasma. An 800 nanometer, 50 femtosecond, 0.35 Watt, 40 KHz, pulsed Ti:Sapphire laser system was used as the source infrared beam. This beam was focused onto a second harmonic generation crystal to produce a collinear, perpendicularly polarized secondary beam at 400 nm. After realigning the polarization of the fundamental to the second harmonic and compensating for group velocity dispersion introduced by the optics, both beams were recombined and focused by a 3.75 cm focal length mirror to form an air plasma. An electrical bias of up to 27 kV/cm was applied across the plasma to enhance the terahertz and plasma signal. The air plasma intensity was measured using a 40 kHz ultrasonic transducer, while the terahertz radiation was measured by a silicon bolometer. Terahertz of reasonable power was detected and characterized using this method. Both the terahertz and the plasma were characterized concurrently throughout this experiment in an effort to determine the feasibility of using the ultrasonic transducer as an alignment aid. The characterization included the effects of polarization, bias, and delay on the plasma and terahertz signals. During the course of this research it was also discovered that silicon, often used as a filter to isolate the detector from the laser in terahertz research, was a significant source of terahertz as well. This experiment represents the first time THz was generated using the two color interaction modified by an external applied bias.

15. SUBJECT TERMS
Index of Refraction, Optical Turbulence, Anomalous Dispersion, Scintillometers, High Energy Laser (HEL), Modeling and Simulation

16. SECURITY CLASSIFICATION OF:			17. LIMITATION OF ABSTRACT	18. NUMBER OF PAGES	19a. NAME OF RESPONSIBLE PERSON
a. REPORT	b. ABSTRACT	c. THIS PAGE			Matthew J. Bohn (ENP)
U	U	U	UU	79	19b. TELEPHONE NUMBER *(Include area code)* (937) 255-3636 x4573 matthew.bohn@afit.edu

Standard Form 298 (Rev. 8-98)
Prescribed by ANSI Std. Z39-18